Natural zeolite clinoptilolite for sustainable energy applications: Insights into water affinity and adsorption properties

Journal of Energy Storage 179 (2026) 123782

Contents lists available at ScienceDirect

Journal of Energy Storage

journal homepage: www.elsevier.com/locate/est

Research papers

Natural zeolite clinoptilolite for sustainable energy applications: Insights into water affinity and adsorption properties

Nadia Grifasi [a], Bianca Ziantoni [a], Alessio Mondello [b], Giuseppe Cruciani [c], Andrea Rizzetto [a], Luca Lavagna [a], Matteo Pavese [a], Fabio A. Deorsola [a], Debora Fino [a], Marco Piumetti [a,*]

[a] Department of Applied Science and Technology, Polytechnic of Turin, Corso Duca Degli Abruzzi, 24, 10129, Turin, Italy
[b] Department of Energy, Polytechnic of Turin, Corso Duca Degli Abruzzi, 24, 10129, Turin, Italy
[c] Department of Physics and Earth Sciences, University of Ferrara, Via Saragat, 1, 44122, Ferrara, Italy

ARTICLE INFO

Keywords:
Natural zeolite
Clinoptilolite
Water affinity
Energy application
Adsorption properties
Sustainable energy

ABSTRACT

Recently, natural zeolites have emerged as promising solutions in the renewable energy sector, offering sustainable solutions and finding applications in several areas. Among them, clinoptilolite stands out for its unique physicochemical properties, low cost, and natural abundance. However, its potential in the energy sector remains largely unexplored. In this study, the performance of natural clinoptilolite and its sodium-exchanged form is evaluated for thermal energy storage and release, focusing on their reversible dehydration behavior and the influence of extra-framework cations on water adsorption capacity. To explore this potential, the samples were characterized using complementary physicochemical techniques, including nitrogen physisorption at −196 °C, X-ray diffraction (XRD), and energy-dispersive X-ray spectroscopy (EDX). Thermal properties were assessed by thermogravimetric analysis (TGA) and differential scanning calorimetry (DSC) to determine mass loss upon heating, enthalpy change, and energy density. Furthermore, FT-IR spectroscopy was employed to gain detailed insights into the interaction of cation-exchanged clinoptilolite with water. Finally, climatic chamber tests were performed to evaluate the water uptake behavior and validate the FT-IR findings. The results indicated that the performance of natural clinoptilolite decreased with increasing sodium content, a trend confirmed by FT-IR spectroscopy and climatic chamber tests. FT-IR spectra revealed variations in peak intensities in both the stretching and bending regions of –OH groups. Clinoptilolite with the highest sodium content (Na/Clino_H) exhibited reduced water affinity, with water desorbing more readily through progressive framework expansion. In contrast, the other samples required thermal activation to achieve desorption, indicating stronger water–zeolite interactions. This behavior is likely related to the elevated sodium content, which appears to hinder water adsorption.

1. Introduction

In recent years, several efforts have been made to address the problem of CO_2 emissions [1–3]. Among them, carbon capture storage (CCS) [4–6] and carbon capture utilization (CCU) [7–13] technologies are noteworthy. The main human activity responsible for that emission is the combustion of fossil fuels (coal, natural gas, and oil), mainly to produce energy and transportation [7,14]. However, several issues derived from CO_2 are well known. This gas is recognized to be the primary driver of climate change, ocean pH variation, and global warming [15–17]. Over the years, the level of CO_2 has increased exponentially. For instance, in 2022, more than 35 billion tons of CO_2 were recorded [15]. This value includes emissions from coal, oil, gas, flaring, cement, steel, and other industrial processes, but excludes land-use change, deforestation, soil, and vegetation. This suggests that the level of these emissions could be higher. Unfortunately, despite the adverse effects on the environment and our planet, fossil fuels are still widely used, mainly in the energy production field, i.e., in the heating and cooling sector. In this context, thermal energy is the widest and most important form of energy, used in several applications, i.e., space heating, water heating, cooking, and other services [18]. However, long-term storage of this energy is challenging due to thermal losses, and its conversion into useful work is often economically unfeasible. Consequently, there has been significant research and financial investment in recent decades

* Corresponding author.
E-mail address: marco.piumetti@polito.it (M. Piumetti).

https://doi.org/10.1016/j.est.2026.123782
Received 29 January 2026; Received in revised form 4 June 2026; Accepted 18 July 2026
Available online 4 August 2026

aimed at transitioning from traditional fossil fuels to renewable energy sources (i.e., solar), in addition to meeting European sustainability targets [18,19]. However, the employment of renewable energy in heating and cooling systems requires innovative and cost-effective solutions due to their seasonal variability [20].

In this context, advanced and sustainable energy storage technologies can address the mismatch in timing between energy demand and peak production [18,21]. In thermal energy storage (TES) systems, the process of charging and discharging during a storage cycle is determined by the materials' capacity to absorb and release heat under specific conditions. These phases are crucial in categorizing TES technologies into three main types: sensible heat storage (SHS), latent heat storage (LHS), and thermochemical energy storage (TCES). Precisely, the last method has gained particular attention, especially for applications at low-medium temperatures (i.e., below 130 °C) [22]. In this case, instead of storing thermal energy in the temperature change (sensible) or change in phase (latent) of the storage medium, thermochemical energy storage systems (also known as sorption thermal energy storage (STES)) employ reversible processes, including physical adsorption and chemical reactions [18,23]. Among the materials investigated, zeolites, MOF, hygroscopic salts, silica-gel, etc., are the most used [18,22,24]. In particular, hygroscopic salts (i.e., $MgCl_2$ and $CaCl_2$) have been widely employed. They possess high thermal energy storage density (400–600 kWh m^{-3}) and are relatively low-cost at $\leq$ USD 500 per metric ton [24]. However, they could melt under certain conditions of temperature and water vapor pressure, resulting in reduced performance of the energy storage system [23].

Zeolites represent an interesting alternative to other materials [25,26]. They are crystalline aluminosilicate materials whose structure consists of interconnected [SiO_4] and [AlO_4] tetrahedra, linked by oxygen atoms, creating an open, crystalline lattice with micropores, where molecules can be trapped [27,28]. Each aluminum atom in the structure imparts a negative charge, which is balanced by exchangeable cations. The type and positioning of these cations within the zeolite structure are essential in determining the material's adsorption properties [22,27]. In TES applications, they are classified as physical adsorbents and are employed thanks to their physico-chemical properties, e.g., thermal stability, ion exchange, reversible rehydration capability, adsorption capacity, and so on [27]. Their use is based on the fact that zeolites can be “charged” by heating and drying, and thermal energy can be recovered later by exposing the dried material to moist air during a “discharging” phase [26,29,30]. Many researchers have focused their attention on synthetic zeolites, mainly 13X, due to their high sorption rate and large sorption capacity [31]. For example, Johannes et al. [32] performed tests by varying flow rates, relative humidity, and hydration temperatures. The experimental results showed that it is possible with their designed open reactor to provide 2250 W during 6 h, namely 27.5 W kg^{-1} of material. In another work, De Antonellis et al. [33] found that performance depends on regeneration temperature, which should be higher than 150 °C. Moreover, the heat storage capacity strongly decreases if air humidification is necessary. To improve the energy storage density, salts (i.e., $MgCl_2$ or $CaCl_2$) or other materials (i.e., graphene) can be introduced into the zeolite matrix or coupled with it to form a composite with enhanced performance, with a high production cost [23,34–36].

In recent years, natural zeolites have garnered significant attention due to their chemical and physical properties, coupled with their economic advantage, as they are derived through natural processes. This makes them an attractive alternative to synthetic zeolites, offering both efficiency and cost-effectiveness [27]. Among them, clinoptilolite gained attention due to its abundance in many countries around the world [37,38]. Hydration and dehydration processes in zeolites have been extensively investigated by water sorption, calorimetry, NMR and high-temperature diffraction studies [39–44]. The presence of extra-framework cations plays a crucial role in governing the interaction strength between water molecules and the zeolite framework, thereby influencing both the amount and reversibility of water uptake. These phenomena are strongly dependent on the type and distribution of compensating cations within the structure. Consequently, hydration properties are considered a key factor in determining the suitability of clinoptilolite for adsorption-based applications. In 2020, Nasruddin et al., [45] conducted a study on the performance of a natural Indonesian zeolite as a potential adsorbent for thermal storage. They observed a temperature increase of 50 °C and an energy storage density of 63.94 kW m^{-3}, which is lower than that of synthetic zeolite 13X or alumina but higher than the values achievable with water or silica gel. This research highlighted the need for further investigation into the use of clinoptilolite for large-scale energy applications, as this mineral demonstrated significant potential.

However, among the studies concerning the use of natural zeolites in the energy field, very few have addressed the comparative evaluation of natural clinoptilolite compared to synthetic zeolite 13X.

Moreover, it was reported that the presence of a specific cation in the framework of zeolite can enhance water adsorption capacity [46]. In particular, divalent cations such as Ca^{2+} and Mg^{2+} exhibit higher hydration energies due to their higher charge density compared to monovalent cations such as NH_4^+ and Na^+, which results in stronger interactions with water molecules and different adsorption behavior within the zeolite framework. Consequently, ion exchange leading to a higher fraction of monovalent cations can modify the distribution and occupancy of extra-framework sites, thereby affecting the accessibility of adsorption sites and the interaction between water molecules and the zeolite framework. However, the relationship between cation composition and water adsorption capacity is not straightforward, as it also depends on the crystallographic location of the cations and the available pore space [44]. Thus, the main aim of this work is to provide a detailed investigation of the thermal properties of the natural zeolite clinoptilolite as a possible alternative to synthetic materials. Although several studies have investigated either the adsorption behavior or the thermal response of natural and synthetic zeolites, a systematic understanding of how compositional variations of extra-framework cations translate into changes in molecular water-zeolite interactions and macroscopic thermal energy storage performance is still limited. In particular, the direct linkage between spectroscopic evidence of adsorption site modification and experimentally measured energy storage metrics remains insufficiently addressed.

Based on these premises, bare clinoptilolite and two Na-exchanged samples with different Na content are investigated and extensively characterized from a thermal point of view by performing TGA, DSC, in situ XRD, FT-IR analysis, and tested in a heated chamber by varying the relative humidity at two different temperatures. Synthetic zeolite 13X is studied for comparison purposes. Specifically, a combined experimental approach is adopted to elucidate how sodium exchange modifies the physicochemical properties of clinoptilolite and, consequently, its water adsorption performance. Structural and compositional information obtained by XRD and EDX was directly related to molecular-level insights from FT-IR spectroscopy, while TGA, DSC and dynamic water sorption measurements were used to quantify the resulting macroscopic adsorption and energy storage behavior. The results of this study could serve as a foundation for evaluating the potential of introducing and further enhancing the use of natural zeolites in the energy sector.

2. Experimental

2.1. Sample preparation

The natural Clinoptilolite sample was provided by the Heiltropfen Lab. LLP company in granular form. Before using, it was grinded to obtain a fine powder and rinsed with ultrapure water to remove some impurities. Subsequently, the sample was dried overnight at 80 °C, and the powder obtained was labeled as “Clino”. To investigate the effect of the amount of sodium in the framework on water affinity, two different

procedures based on ion exchange were adopted to obtain the required loading. This was made because the procedure adopted for low Na-loading was not sufficient to achieve the high sodium content required in high Na-loading zeolite.

Specifically, to get Clinoptilolite with low Na-content, the cation-exchange procedure proposed by Davarpanah et al. [5] was followed with some modifications. Briefly, a suitable amount of NaCl, used as a precursor, was dissolved in ultra-pure water at room temperature. After that, the temperature was increased up to 50 °C, and the Clino powder was added to the solution, maintaining the stirring for 2 h. At the end, the sample was recovered, rinsed with water, and centrifuged three times. Finally, it was dried for 24 h at 65 °C and subsequently calcinated at 550 °C for 4 h with a ramp of 2 °C min^{-1}. The sample obtained was labeled as "Na/Clino_L".

In the case of a higher Na-content sample (Na/Clino_H), the procedure suggested by Crocellà et al. [4] was adopted with slight modifications. Firstly, Clino powder was exchanged with $(NH_4)_2SO_4$ under stirring at 90 °C to obtain NH_4-exchanged Clino, which can lead to higher exchange with sodium. After 2 h, the sample was centrifuged, and this step was repeated a second time before drying at 125 °C overnight. The second step consisted of obtaining a Na-exchanged sample by using a $NaNO_3$ 0.5 M solution as a precursor and leaving the powder under stirring for 18 h at 60 °C. In the end, it was centrifuged, and the second step was repeated twice. Finally, the powder was dried at 100 °C overnight and then calcinated under the same conditions as the Na/Clino_L sample to obtain the sample labeled "Na/Clino_H".

For comparison purposes, the commercial 13X synthetic zeolite was also investigated.

2.2. Sample characterization

The Specific Surface Area (SSA, $m^2\ g^{-1}$) and total pore volume (VTP, $m^3\ g^{-1}$) were evaluated through N_2-physisorption at −196 °C in a Micromeritics Tristar II 3020 apparatus (v1.03, Micromeritics Instrument Corp., Norcross, GA, USA). The samples were outgassed by feeding N_2 at 200 °C for 2 h to remove any adsorbed contaminants and moisture on the surface. The SSA and VTP were estimated with the Brunauer-Emmett-Teller (BET) method and Barrett-Joyner-Halenda (BJH) method during the desorption phase, respectively.

The crystalline phase was studied through powder X-ray diffraction (XRD) using a Panalytical X'Pert PRO PW3050/60 diffractometer (Malvern Panalytical Ltd., Malvern, UK) equipped with a PIXcel-1D detector and copper tube. The XRD data were collected over the 2θ angle range of 5–65° with a step size of 0.026° and an equivalent time per step of 60 s. The collected patterns were interpreted with reference to the Powder Diffraction File database (PDF-2004, International Centre for Diffraction Data) and modeled by the Rietveld method using the Bruker-AXS TOPAS program to obtain quantitative phase analysis. For each identified crystalline phase, the scale factor was refined together with the background, profile parameters and unit-cell parameters. The refined scale factors were then converted into weight fractions according to the standard Rietveld relationship

$$W_p = S_p(ZMV)_p \Big/ \sum_i S_i(ZMV)_i$$

where S_p is the refined scale factor and Z, M, and V are the number of formula units per unit cell, the mass of the formula unit, and the unit-cell volume of phase p, respectively. The summation in the denominator is extended to all crystalline phases i included in the refinement. Thus, the calculated values correspond to normalized crystalline phase fractions obtained from the refined scale factors. Possible amorphous content was not quantified because no internal standard was used.

XRD measurements were also carried out in situ to investigate the effect of temperature on the crystal structure. Data collection was performed on a Panalytical Empyrean (Panalytical, Almelo, The Netherlands) diffractometer equipped with a PIXcel-1D detector. The samples were heated in HTK1200N under an air atmosphere, increasing the temperature from room temperature up to 700 °C. The collected patterns were analyzed by the Rietveld method to determine the variation of cell parameters.

EDX analysis was performed on a Talos Thermo Scientific instrument equipped with a LaB_6 gun to evaluate the atomic percentage of all the cations present in the samples. In a typical procedure, a small amount of powder was dispersed in pure isopropanol, sonicated for 15 min at room temperature, and deposited on copper grids equipped with lacey carbon films. The data were acquired in three different areas to verify the homogeneity of the material.

Thermal properties and stability in a wide range of temperatures were also investigated. Differential scanning calorimetry (DSC) was carried out to evaluate the quantity of heat exchanged by the samples undergoing a physical and/or chemical transformation. A Perkin-Elmer Pyris 1 Heat-Flux differential scanning calorimeter, working in an N_2 atmosphere, was used for this purpose. Specifically, to evaluate the enthalpy of adsorption (ΔH, J g^{-1}), the samples were first completely saturated with moisture and, subsequently, introduced into the DSC chamber where the temperature started to increase from 30 °C to 350 °C, with a heating rate of 10 °C min^{-1}. The enthalpy of adsorption was then used to calculate the energy density of the material as follows [18]:

$$ED = \frac{\Delta H}{m}$$

Where ΔH is the enthalpy of adsorption (J), while m (g) is the mass of the sample.

Additionally, thermo-gravimetric analysis (TGA) was conducted with a TGA instrument, Mettler Toledo TGA / DSC 3+. All the samples were heated from 30 °C to 700 °C with a constant heating rate of 10 °C min^{-1} by flowing 50 ml min^{-1} of air.

2.3. Water affinity tests

FT-IR spectroscopy was employed to deeply investigate the water affinity. The analyses were carried out on a Bruker INVENIO instrument equipped with a liquid nitrogen-cooled MCT detector by following the procedure described in the literature [7,47,48]. A small quantity of powder was pressed into a thin disc and placed in a quartz IR cell equipped with KBr optical windows. Each sample was degassed at 10^{-4} mbar and pretreated at 400 °C for 4 h by connecting the IR cell to a high vacuum line. Subsequently, the system cooled down to room temperature, and water was fed into the IR cell at different partial pressures (from $9 \cdot 10^{-4}$ to 1 mbar) to investigate the hydrophilicity and water affinity. Spectra were recorded at room temperature in transmittance mode in the region ranging from 4000 to 400 cm^{-1} with a resolution of 4 cm^{-1}. The entity of adsorption was evaluated by normalizing the spectra with respect to both the superficial density and the maximum intensity of the peak. The adsorption step was followed by gradual expansions consisting of progressive degassing over time (0–60 min) to check the possibility of desorbing water by a simple pressure reduction, without thermal treatment.

To evaluate the water uptake of the samples, a gravimetric dynamic water sorption analysis was performed using a SPSx-1 μ High Load instrument manufactured by ProUmid in Germany. This device can accommodate up to 23 samples simultaneously, enabling their analysis under identical experimental conditions. Prior to the measurements, the samples were dehydrated in an oven at 120 °C for 24 h. After drying, they were placed inside the instrument, and their initial mass was recorded. A complete water sorption and desorption isotherm at 30 °C was then obtained by exposing the samples to a series of relative humidity (RH) levels from 10% to 90% and back to 10%, with steps of 10%. At each RH step, the mass of the samples was recorded every 10 min to track water uptake. The water uptake was determined by measuring the

equilibrium mass at each RH level, assuming equilibrium had been reached when the change in sample mass during the last 40 min was lower than 0.01%. The RH level was changed only after all samples had reached equilibrium at the current step. The resulting data correspond to water adsorption and desorption isotherms at 30 °C.

2.4. Key performance indicators (KPIs) evaluation

Key Performance Indicators (KPIs) are essential parameters used to evaluate and compare the performance of different technological solutions within a specific scientific context. Among the most commonly used KPIs in energy storage applications, in this work, particular attention was given to the cost factor, which was analyzed in terms of Storage Capacity Cost (SCC, € kWh^{-1}). This parameter is especially relevant when comparing the economic feasibility of different storage materials or systems and was calculated using the following Eq. [18]:

$$SCC = \frac{€/\text{ton}}{ED}$$

This formula links the material cost per ton to its energy density (ED, GJ ton^{-1}) and provides a clear metric for assessing how much it costs to store one kilowatt-hour of energy.

3. Results and discussion

3.1. Physico-chemical characterization

The adsorption-desorption isotherms from N_2 physisorption at −196 °C are shown in Fig. 1, whereas Table 1 summarizes the values of the SSA and VTP for all the investigated materials. Concerning the natural zeolites, the isotherms exhibited a hysteresis loop within the 0.6–1 P/P^0 range, and the shape can be ascribed to a type IV B or type H3 isotherm, according to the IUPAC classification. This type of hysteresis is commonly observed in natural zeolitic materials and is typically associated with non-rigid aggregates of plate-like particles or the presence of slit-shaped voids arising from particle packing rather than well-defined mesoporous channels [49]. It is also important to emphasize that ion exchange does not affect the zeolite framework and consequently the SSA, but it just modifies the hydration energy, the cation exchange capacity, as well as the affinity toward target molecules, according to the properties of the exchanged cation [50]. Therefore, a change in the hysteresis type loop is not expected between natural and modified natural zeolite. Moreover, other adsorption measurements reported in the literature for HEU-type zeolites [4] have shown that, even when alternative probe molecules are used to access ultramicroporous regions, such as CO_2, the overall adsorption behavior remains strongly governed by framework accessibility and cation distribution rather than by changes in pore architecture. Therefore, the observed differences in adsorption features are more appropriately attributed to morphological and energetic effects rather than to structural mesopore formation. Moreover, given the low specific surface area of clinoptilolite-based samples, the observed adsorption behavior could be related to interparticle voids and structural heterogeneity typical of natural mineral aggregates.

Table 1
Textural properties of the prepared and commercial zeolite calculated from N_2 physisorption at −196 °C.

Sample	SSA [a] (m^2 g^{-1})	Vp [b] (cm^3 g^{-1})	microporous area [c] (m^2 g^{-1})	microporous volume [c] (cm^3 g^{-1})
Clino	25.7	0.119	5.1	0.003
Na/Clino_L	20.5	0.122	1.4	0.001
Na/Clino_H	25.5	0.083	1.3	0.001
13X	526.9	0.130	474.3	0.2221

[a] Specific surface area (SSA) evaluated according to the Brunauer–Emmett–Teller (BET) method.
[b] Total Pore Volume (VTP) evaluated according to the Barrett–Joyner–Halenda (BJH) method during the desorption phase.
[c] Micropore area and micropore volume evaluated from t-plot.

The 13X isotherm resembled the typical type-I isotherms, and this was consistent with the literature [51,52].

Not only the shape of the isotherms but also the surface area values showed significant differences between natural zeolites and the synthetic one. Specifically, Clino (both in its natural and exchanged form) presented an extremely low surface area, ranging between 20 and 25 m^2 g^{-1}. This value was much lower compared to that of synthetic zeolites like 13X, which typically exhibited higher surface areas (526.9 m^2 g^{-1}). Furthermore, the micropore area and micropore volume evaluated from the t-plot confirmed that 13X exhibited a higher fraction of micropores compared to the natural zeolites. Moreover, the higher the concentration of sodium, the lower the micropore area. This could be due to the higher amount of sodium, which probably tends to hinder N_2 access to narrower microporous cavities. This finding was consistent with the literature [27,53] and can be attributed to the fact that Clino and Na/Clino are natural zeolites, whereas synthetic zeolites are obtained through highly controlled and precise conditions (temperature,

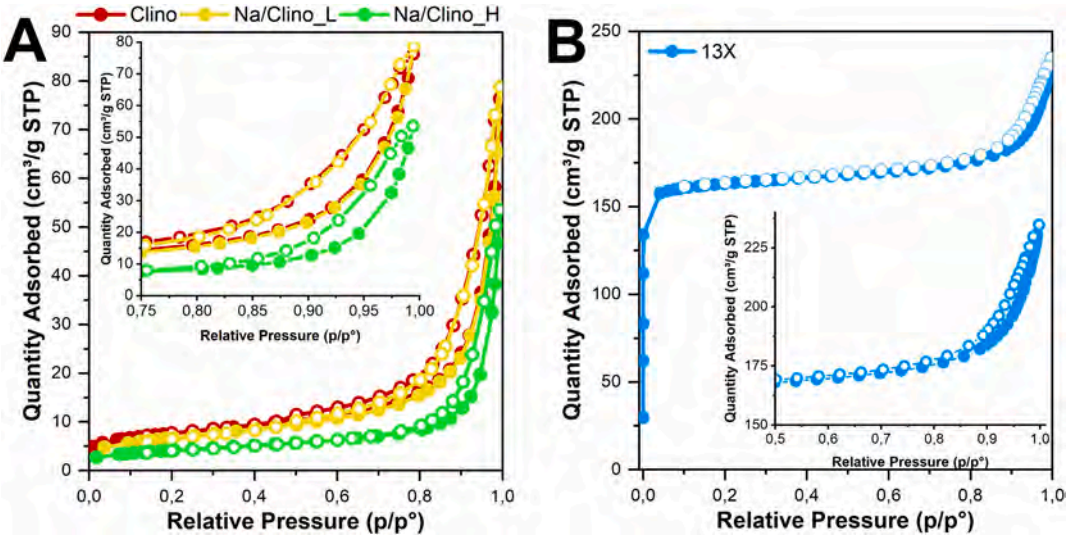

Fig. 1. N_2 isotherms of the Clinoptilolite-based materials (A) and commercial 13X (B).

pressure, use of templates, etc). Additionally, ion exchange with Na^+ ions does not significantly affect the specific surface area, as it does not alter the zeolite framework structure but only involves the substitution of extra-framework cations [50]. Therefore, only minor variations in SSA may be observed, typically within the experimental uncertainty of nitrogen physisorption measurements. Moreover, the low surface area reflected the diverse conditions that can be found in nature, which depend on the deposit. In fact, due to the different geological conditions during their formation, a high degree of heterogeneity can influence the SSA and overall properties, i.e., chemical composition. However, it should be noted that the relatively low specific surface area of clinoptilolite-based materials is not solely related to their natural origin, but rather to their HEU-type framework topology, the presence of minor mineral impurities, and partial blocking or limited accessibility of microporous channels, which can reduce the measured N_2-accessible surface area.

To validate this assumption and confirm that ion exchange effectively occurred, an EDX analysis was performed, and the results are reported in Fig. 2.

As a whole, the Clino sample exhibited the presence of different cations, whose percentage depends on the deposit and geographical area. Precisely, in addition to Si, Al, and O elements, which are the constituents of a zeolitic mineral, the presence of a multitude of cations was also detected, such as Na, Mg, K, Ca, and Fe. This finding was consistent with previous reports [5,6,54] but contrasted with the behavior of synthetic zeolite 13X, which is produced under controlled conditions to ensure structural uniformity. In fact, only the sodium as a cation was detected, with an atomic concentration of 14.4%. Concerning the natural samples, both Clino and the two Na-exchanged samples (Na/Clino_L and Na/Clino_H) exhibited similar percentages of Si, O, and Al, which are the main constituents of the alumino-silicate structure. On the other hand, after the ion-exchange process, the increase in Na content was accompanied by a progressive decrease in the concentration of the original extra-framework cations present in the Clino sample. This suggested the effectiveness of the procedures adopted to obtain Na/Clino_L and Na/Clino_H. Specifically, regarding the sodium content, the results highlighted that Clino presented 0.7 at.% of Na, whereas Na/Clino_L contained 2.8 at.%. % with a standard deviation of 0.015%, while the sample Na/Clino_H exhibited a higher percentage of sodium compared to the others, equal to 5.7 at. % with a standard deviation of 0.57%. Moreover, the higher the sodium content, the lower the amount of the other cations detected with respect to the bare Clino (i.e., Mg, K, Ca, Fe). In particular, calcium showed the largest decrease after Na exchange, followed by potassium, magnesium, and iron species. For the highly exchanged sample (Na/Clino_H), Ca decreased by approximately 78%, K by 63%, Mg by 75%, and Fe by 33% compared to untreated Clino. Similar but less pronounced variations were observed for Na/Clino_L, with 89% for Ca, 50% for K, and Fe by 17% for Fe. No variation was detected for Mg concentration. These results suggested that Ca-containing sites are among the most affected by the exchange treatment. According to previous structural studies on clinoptilolite, different extra-framework cations occupy distinct positions and coordination environments within the zeolitic channels, resulting in different ion-exchange behaviors and selectivity [4,27]. Therefore, the observed compositional variations were consistent with the intrinsic cation selectivity of clinoptilolite. The findings confirmed that both procedures adopted were suitable to obtain different percentages of sodium, in line with the purpose of the work. These compositional variations were expected to directly influence the distribution and strength of water adsorption sites, thereby affecting the hydrophilicity and subsequent thermal energy storage behavior of the materials.

The XRD results for phase identification and quantification revealed that the natural clinoptilolite-containing sample (Fig. 3A) was composed of about 90 wt% zeolite, 8 wt% silica phases (quartz and tridymite), and 2% K-feldspar. The phase fractions of Clino were maintained in Na/Clino_L, while a minor decrease of the zeolite content was found in Na/Clino_H. A direct comparison of powder patterns showed that ion exchange treatments did not cause any substantial alteration in the zeolite framework structure except in the unit cell dimensions. The unit cell volume of clinoptilolite, calculated from the Rietveld-refined monoclinic unit cell parameters, changed from about 2092 $Å^3$ in Clino to 2088 $Å^3$ in Na/Clino_L $Å^3$, to 2097 $Å^3$ in Na/Clino_H, as a result of the Na-exchange treatments. The variation in the occupancy of the zeolite extra-framework sites was also revealed by a change in the relative

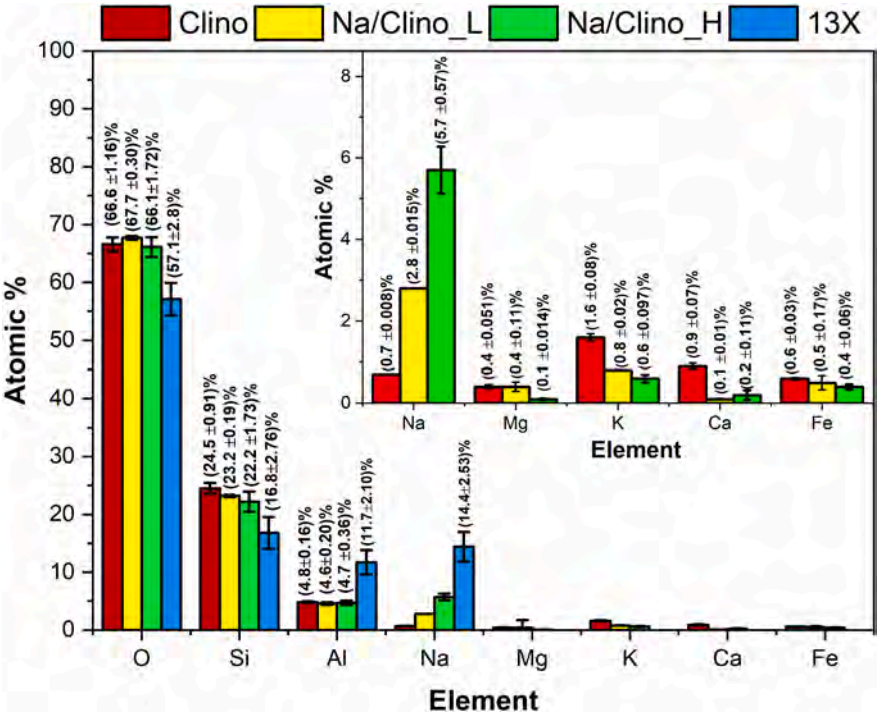

Fig. 2. Chemical composition of the natural zeolite samples and 13X obtained from EDX analysis.

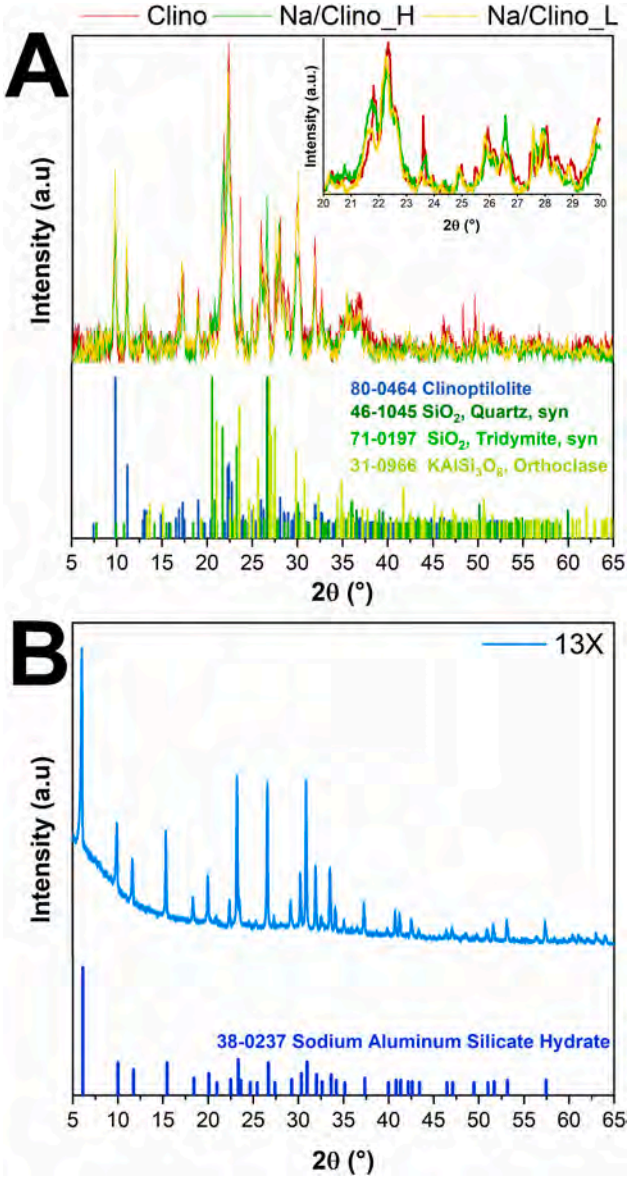

Fig. 3. Diffraction patterns of bare and Na-exchanged Clino samples (A) and 13X (B).

intensity of the (040) peak located at approximately 2θ = 19.8° (Cu Kα radiation), in agreement with the literature [55].

The phase identification and Rietveld analysis of the powder XRD pattern of zeolite 13X (Fig. 3B) showed the absence of detectable impurities, and the refined cubic unit cell parameter was 24.98 Å, in perfect agreement with the 24.99 Å value known for the NaX zeolite.

Besides the difference in the framework topology and channel system geometry of the two zeolites considered in this study, the XRD analyses clearly highlighted the well-known fundamental variance between natural and synthetic zeolite materials: impure and less crystalline the former, while pure and more crystalline the latter.

On the other hand, both clinoptilolite and zeolite 13X are generally recognized for their high thermal stability, although the actual framework stability strongly depends on factors such as framework topology, Si/Al ratio, and the nature of the extra-framework cations, as reported by Cruciani [56]. In particular, the author reported breakdown temperatures of approximately 900–1070 °C for several clinoptilolite forms, depending on the exchanged cation (e.g., about 920 °C for Na-clinoptilolite, about 1000 °C for K-clinoptilolite, about 1070 °C for Cs-clinoptilolite, and about 900 °C for Ca-clinoptilolite). In order to assess the thermal stability of the samples used in this study, an in situ XRD analysis was performed for all the samples investigated (Fig. 4, Fig. 5 and **Fig. S1**). Precisely, Fig. 4**A** and **C** report the complete in situ XRD patterns collected over the investigated 2θ range for Clino and zeolite 13X, respectively, whereas Fig. 4**B** and **D** show magnified views of the low-angle regions containing the most representative zeolitic reflections, in order to better visualize peak shifts and structural variations upon heating. The in situ XRD study confirmed that both the natural and synthetic zeolite samples used in this investigation exhibited excellent thermal stability. Specifically, under the experimental conditions adopted in this work, all the materials maintained their crystalline structure up to 700 °C.

The in situ XRD study confirmed that both the natural and synthetic zeolite samples used in this investigation exhibited excellent thermal stability, showing no significant changes in their crystalline structures throughout the temperature range. In the case of the Clino sample, the increasing shift of zeolite peaks to higher 2θ angles (narrower *d*-spacing) was the consequence of the unit cell shrinkage due to loss of the channel water molecules, whereas this behavior was less pronounced in zeolite 13X. In Fig. 6, the variation of Rietveld-refined unit cell volume as a function of temperature is compared for the two zeolites under investigation. Clino exhibited volume contraction in the RT-450 °C range, with the largest decrease of about 3.4% at 500 °C. In contrast, zeolite 13X showed the largest volume contraction of about 0.2% at 100 °C, while the thermal expansion explained the volume increase at higher temperatures. Zeolite 13X almost fully regained its original unit cell volume at RT after heating, while Clino regained 98.8% of the initial unit cell volume. The different thermal behavior of the two zeolites can be rationalized considering the collapsible nature, with co-rotating hinges, of the HEU framework topology of Clino, while the FAU topology of zeolite 13X framework behaves as non-collapsible with anti-rotating hinges [56].

To further investigate the dehydration behavior of the two samples, TGA analysis was performed. This analysis was also carried out on samples of Clino and zeolite 13X, to allow for a comparison with the raw material and with the gold standard for this type of application, respectively. The results are reported in Fig. 7.

Previous TGA/DSC and high-temperature XRD studies on zeolites have shown that water removal occurs in distinct temperature ranges, broadly corresponding to weakly adsorbed water, cation-coordinated/channel water, and high-temperature dehydroxylation or structural water loss, depending on framework topology and cation composition [56,57].

More precisely, at low temperatures (between 50 °C and 150 °C), the weakly physisorbed water on the zeolite surface (weakly bonded water) is lost. Between 150 °C and 250 °C, water present inside the zeolitic cavities and water bound to extra-framework cations is released. Finally, above 450 °C, the so-called structural water is lost, which leads in some cases to collapse and the eventual breakdown of the zeolitic framework, while in other cases leaves the zeolite almost unaffected up to very high temperatures [56,58,59]. From the TGA analysis, the amount of water lost upon heating was found to decrease in the following order: 13X > Na/Clino_L > Clino > Na/Clino_H. In particular, the Clino and Na/Clino_H samples exhibited similar profiles, each showing a small peak between 50 °C and 150 °C corresponding to approximately 5% mass loss. The Na/Clino_L sample also displayed a peak within a similar range (50 °C–100 °C), slightly shifted toward higher temperatures (centred around 75 °C), but with a water loss approximately twice that of the previous samples, reaching about 10%. The observed differences in water loss among Clino, Na/Clino_L, and Na/Clino_H suggested that the dehydration behavior is not directly proportional to the sodium content, but rather depends on the balance, distribution, and accessibility of extra-framework cations within the clinoptilolite structure [60]. In zeolitic systems, water molecules interact with charge-balancing cations located at specific framework sites, and their coordination strength varies depending on the nature and location of these cations.

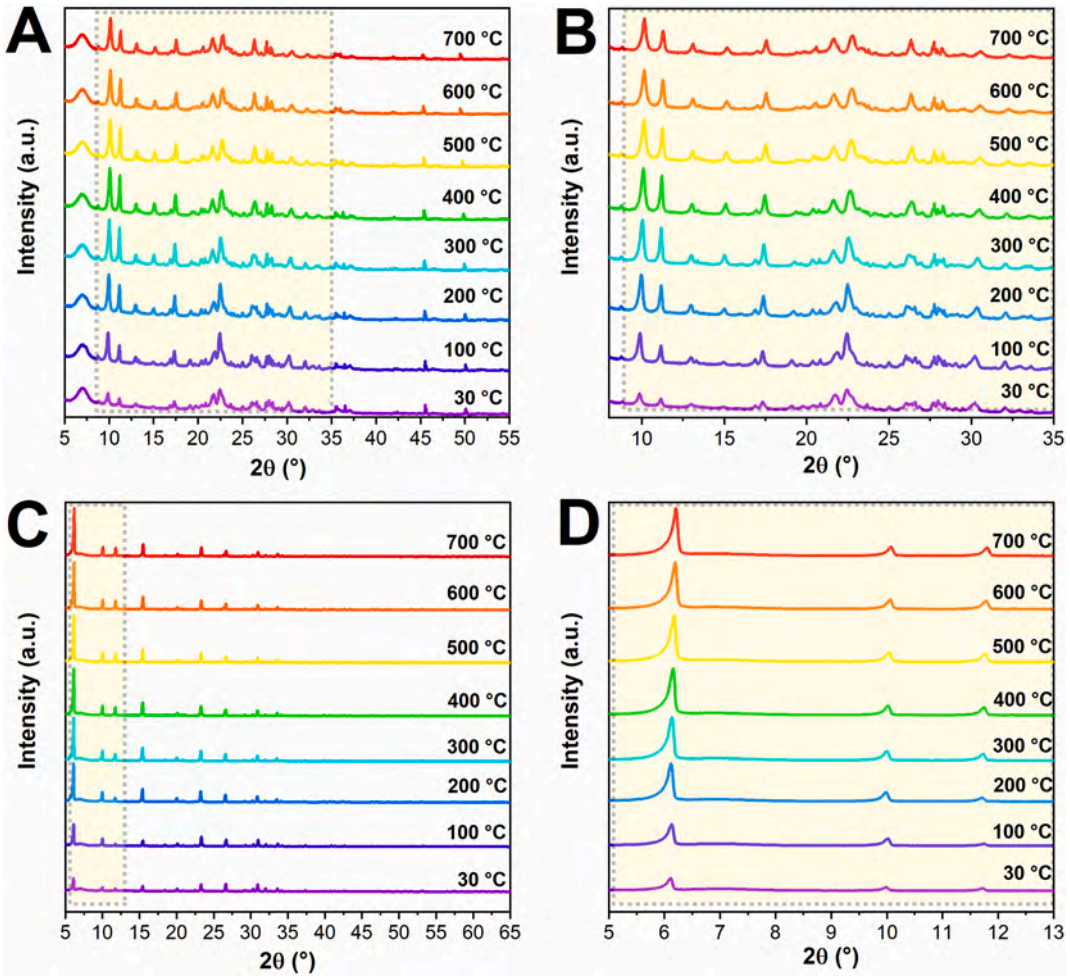

Fig. 4. In situ XRD patterns of bare Clino and 13X during heating from room temperature to 700 °C: (A) full 2θ range for Clino; (B) magnification of the low-angle region for Clino; (C) full 2θ range for 13X; (D) magnification of the low-angle region for 13X.

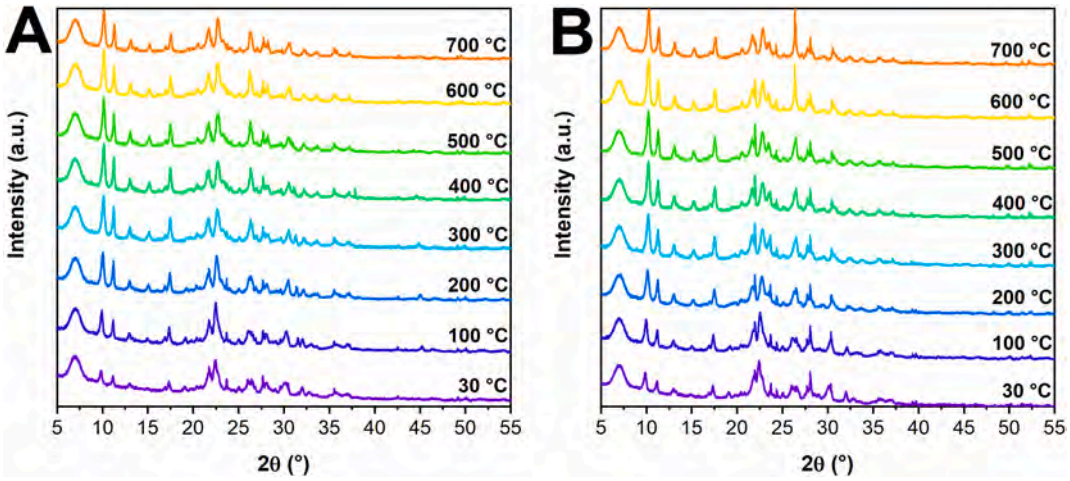

Fig. 5. In situ XRD patterns of Na/Clino_L (A) and Na/Clino_H (B) during heating from room temperature to 700 °C.

Monovalent (e.g., Na^{+}, K^{+}) and divalent cations (e.g., Ca^{2+}, Mg^{2+}) differ in their hydration strength and coordination environment, which in turn affects the stability of adsorbed water species. As a consequence, variations in the relative abundance of these cations can lead to differences in the number and strength of water adsorption sites. In this context, the higher water loss observed for Na/Clino_L can be attributed to a more favourable balance between exchanged Na^{+} ions and residual native cations, which promotes a greater number of accessible adsorption sites. Conversely, in Na/Clino_H, the higher degree of sodium exchange may reduce the contribution of other strongly hydrating cations, leading to a lower overall water retention. Therefore, the dehydration behavior reflects a combined effect of cation type, distribution, and site occupancy

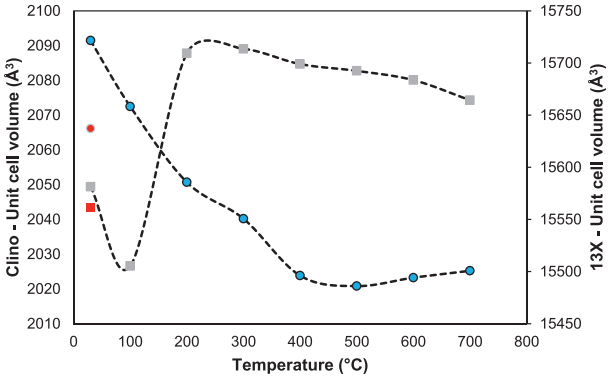

Fig. 6. Variation of the unit cell volume as a function of temperature for Clino (circles) and zeolite 13X (squares). Red symbols are for measurements at RT after heating up to 700 °C

rather than Na^+ content alone.

The observed trend confirmed that the structural modifications induced by sodium exchange directly influenced the number and strength of adsorption sites available for water molecules, which was reflected in both the thermal dehydration behavior and the resulting energy storage density, as reported in the following sections. Finally, the 13X zeolite exhibited the highest water loss, approximately 20%, over a broader thermal range of 50 °C to 250 °C. The ~21% maximum water loss of zeolite 13X compared to the ~10% of Clino reflected once again the difference in framework density, which is a major control on the maximum water adsorption capacity of any specific framework topology. It was also noteworthy that zeolite 13X topology was able to withstand the largest water loss with minimal contraction of the unit cell volume due to the non-collapsible nature of its tetrahedral framework, as pointed out previously.

The DSC profiles revealed a strong endothermic signal extending over a broad temperature range between 25 °C and 250 °C, attributed to the desorption of water adsorbed within the microporous structure of all the samples investigated. For the Clino and Na/Clino_H samples, a similar broad endothermic peak was observed between 30 °C and 200 °C. This similarity closely mirrored that seen in their respective TGA curves. In contrast, the Na/Clino_L sample exhibited a more intense and narrower endothermic peak between 30 °C and 100 °C, centered at approximately 75 °C, corresponding to the water desorption event observed in the TGA profile. This peak was followed by a tail extending the thermal range up to approximately 200 °C, aligning with the behavior of the previously mentioned samples. In the case of the 13X sample, the endothermic peak displayed a minimum heat flow value comparable to that of the Na/Clino_L sample, but with a broader temperature range extending from 30 °C to 250 °C. A shoulder can be identified between 30 °C and 100 °C, likely associated with the release of more weakly bound water. According to literature [56], such features were consistent with the presence of surface or loosely adsorbed water, while higher-temperature peaks are indicative of more strongly adsorbed or deeply confined water molecules. The main endothermic peak for 13X was centred at around 160 °C. Overall, the DSC curves were in good agreement with the TGA results. Additionally, the dehydration enthalpy (ΔH, in J g^{-1}) was estimated from the DSC curves for all samples and was reported in Table 2. The trend of increasing endothermic response followed the order: Na/Clino_H < Clino < Na/Clino_L < 13X. These results were consistent with previously published findings [56,61], although it should be noted that the baseline definition for peak integration remained a challenging aspect of the analysis.

3.2. Dynamic vapor sorption (DVS) analysis

The adsorption/desorption isotherms at 30 °C, obtained simultaneously for all the materials, are shown in Fig. 8. The curves obtained revealed that Na/Clino_L exhibited a different behavior compared to the others.

Following the IUPAC classification [61], Zeolite 13X, Clino, and N-

Table 2
Results of TGA and DSC measurements of all the samples investigated.

Sample	Temperature Peak range[a] (°C)	Mass loss[b] (%)	$\Delta H_{(25-250°C)}$[a] (J g^{-1})
Clino	50–150	9.9	114.3
Na/Clino_L	50–100	15.1	176.5
Na/Clino_H	50–150	9.1	75.9
13X	50–250	21.3	364.6

[a] value evaluated from DSC.
[b] Value evaluated from TGA.

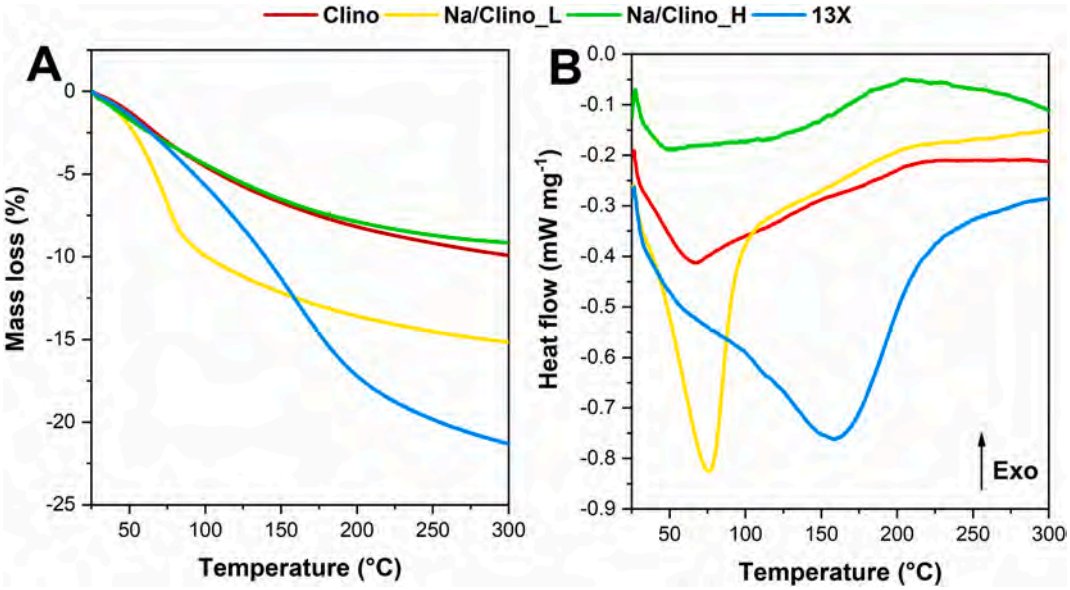

Fig. 7. TGA curves of all investigated samples in the temperature range between 25 °C and 300 °C (A) and DSC experimental results for hydration enthalpy evaluation (B).

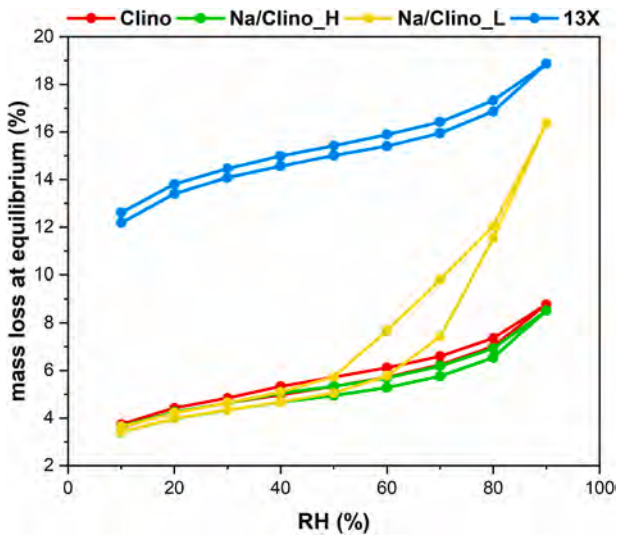

Fig. 8. Adsorption/desorption isotherms obtained at 30 °C. The x-axis represented the relative humidity (RH %), while the y-axis showed the percentage change in water content relative to the initial mass of the sample after dehydration at 120 °C. This value corresponded to the ratio, expressed as a percentage, between the mass of adsorbed water at equilibrium and the initial mass of the sample after dehydration.

Clino_H displayed a type I isotherm. The very small difference between the adsorption and desorption branches should not be attributed to hysteresis, but rather to the type of analysis and the conditions employed. The tendency of the curves to rise at higher relative humidity (RH) without reaching a stable asymptotic value should also be explained by the measurement conditions, considering that the ambient pressure and temperature within the climatic chamber favoured water condensation. Moreover, the presence of small aggregates within the fine powder can generate interparticle macropores, where water may easily condense under these conditions, thus simulating a type II isotherm behavior in the final part of the curves.

The Na/Clino_L sample, on the other hand, exhibited a type IV isotherm. This was characterized by initial monolayer adsorption within micropores, followed by capillary condensation in mesopores. The hysteresis loop, according to the IUPAC classification [61], can be identified as either an H3 or H4 type. The latter was more appropriate, considering the significant water uptake observed in the initial part of the isotherm, as well as the fact that H4 loops were typically associated with zeolites forming aggregated crystals or with mesoporous zeolites [61]. This specific isotherm shape suggested that Na-enrichment in this sample promoted the development of a mesoporous network, which was not observed in either the raw material or the more enriched Na/Clino_H sample. It should not be interpreted as evidence of true mesoporosity generated by ion exchange, but rather as the result of textural effects, particle aggregation/interparticle voids, and changes in water adsorption energetics/accessibility. Such a mesoporous structure resulted in a significantly enhanced water uptake at high RH levels. Indeed, up to 50% RH, all three Clino samples exhibited similar water uptake behavior, whereas beyond this point, the Na/Clino_L sample showed a marked increase, reaching 16.4% water uptake, compared to about 8.8% and 8.5% water uptake, respectively, for both the Clino and Na/Clino_H samples. Zeolite 13X, indeed, exhibited a faster growth of the isotherm at low RH% and a better final uptake, of about 18.9%.

Finally, the water uptakes for all the samples were in accordance with the results obtained for water loss in the TGA. The differences observed in the adsorption isotherms can therefore be directly correlated with the structural and compositional changes identified by EDX and FT-IR analyses (see later), confirming that sodium content played a key role in tuning the hydrophilic behavior of clinoptilolite-based samples.

Moreover, a consistent correlation between water adsorption behavior, hydrophilicity, and thermal energy storage performance can be established by combining DVS, TGA, and DSC results. Higher water uptake corresponded to a greater number of active adsorption sites, leading to increased dehydration enthalpy measured by DSC and, consequently, higher energy density. Conversely, reduced water adsorption resulted in lower hydrophilicity and lower thermal energy storage performance. Among the investigated samples, Na/Clino_L exhibited the highest water uptake and thus the highest dehydration enthalpy among natural zeolites, while Na/Clino_H showed the lowest values, confirming that excessive sodium exchange reduces adsorption efficiency.

These trends are further reflected in the Key Performance Indicators (KPI) discussed in Section 3.4, where higher energy density results in lower Storage Capacity Cost (SCC), highlighting the direct link between hydrophilicity and economic performance of the material.

3.3. *In situ FT-IR investigation*

In order to gain a better understanding of the affinity of water with the zeolite materials and the influence of Na, in situ FTIR experiments were performed. As reported in the *Materials and Methods* section, all the materials were first pretreated at 400 °C in a vacuum line to eliminate the interference of the hydration. The full spectra after the pretreatment were reported in Fig. S2.

Detailed magnifications of the hydroxyl stretching region and the 2250–1500 cm^{-1} spectral range are depicted in Fig. 9. Regardless of the zeolite type, all zeolites exhibited a sharp peak with a maximum around 3746 cm^{-1}, which can be attributed to the presence of isolated Si-OH groups located on the external surface of the zeolites [7,62,63].

Pristine clinoptilolite zeolite displayed a relatively broad band at 3581 cm^{-1}, which has been previously associated with bridging hydroxyl groups in zeolitic systems [62–65]. However, contributions from hydroxyl species generated during the thermal pretreatment at 400 °C cannot be excluded. The maximum of this band shifted to a higher wavenumber (3628 cm^{-1}) when the material was exchanged with Na^+ ions, as observed for the Na/Clino_L and Na/Clino_H samples. In parallel, the relative intensity of this band decreased with increasing sodium exchange, suggesting that sodium exchange altered the local environment of hydroxyl species associated with the zeolite framework [62].

The structure of faujasite-type zeolite (13X) consists of cages of two different sizes (supercages and sodalite cages). The hydroxyl-related absorptions observed for zeolite 13X are consistent with OH species commonly reported for FAU-type zeolites, possibly including defect or non-bridging hydroxyl groups generated or exposed during thermal pretreatment [63,66]. In particular, the bands around 3691 cm^{-1} (HF region) and in the 3500–3300 cm^{-1} range (LF region) have been previously associated with hydroxyl species located in the supercages and sodalite cages, respectively. However, considering the Na-rich nature of the investigated 13X sample and the thermal pretreatment applied, the contribution of non-bridging or defect hydroxyl species cannot be excluded.

At lower wavenumbers (2200–1500 cm^{-1} range), the spectra of clino-based zeolites exhibited the contribution of framework modes, i.e., overtones of n(T—O—T), with a maximum at 1874 cm^{-1} [62–64].

Between 1644 and 1630 cm^{-1}, a band corresponding to the bending mode of the OH bond (δOH) was observed, which was attributed to residual hydration despite vacuum thermal treatment [5,67–69].

Zeolite 13X exhibited an absorption band centered at 1577 cm^{-1}, which can be related to strongly adsorbed carbonates on the material's surface [63]. The relative intensities of the framework modes, as well as the band at 1641 cm^{-1}, decreased with increasing sodium content in clinoptilolite-based materials, likely due to saturation and/or pore coverage by sodium species.

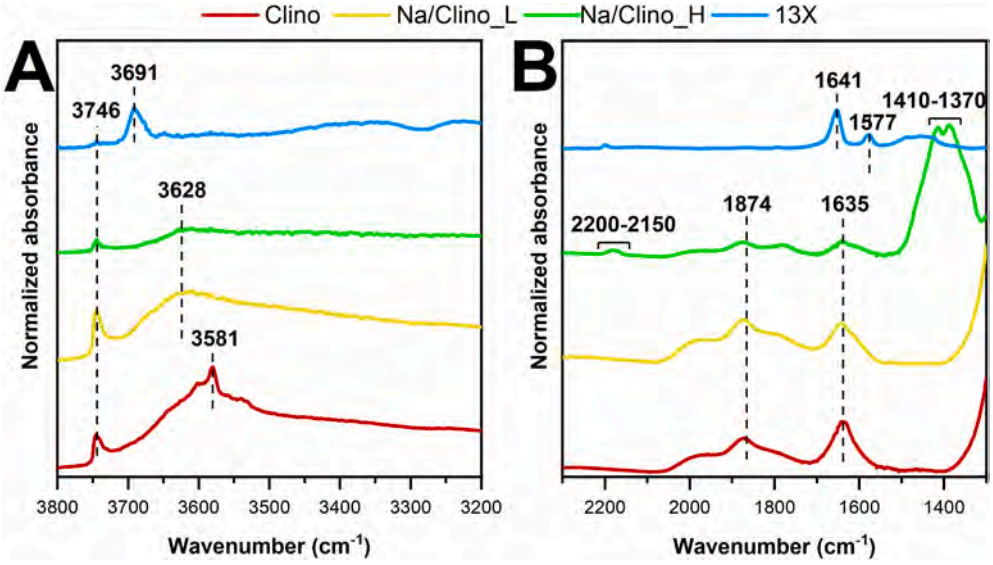

Fig. 9. FT-IR spectra of the pretreated samples of -OH stretching region (3800–3200 cm^{-1}) (A) and -OH bending region (2300–1300 cm^{-1}) (B).

Additional absorptions in the 2200–2150 and 1410–1370 cm^{-1} regions were observed for Na/Clino_H. The band at 1410–1370 cm^{-1} is consistent with surface carbonate species, likely formed upon exposure to atmospheric CO_2. The feature at 2200–2150 cm^{-1} may arise from combination bands of adsorbed CO_2 species and/or NOx-derived surface species associated with the $NaNO_3$ precursor [70].

A study by Szanyi et al. [71] reported absorptions within the same spectral ranges during investigations of NO_2 adsorption on Na—Y. Specifically, the band observed between 2200 and 2150 cm^{-1} was attributed to the vibration of an NO^+NO_2-type adsorption complex. This interpretation aligned with findings from a study by Khivantsev et al. [72] on nitrate-containing zeolites, where an asymmetric absorption around ~2195 and ~ 2171 cm^{-1} was ascribed to two NO^+ stretches. Furthermore, the doublet feature within the 1350–1450 cm^{-1} range

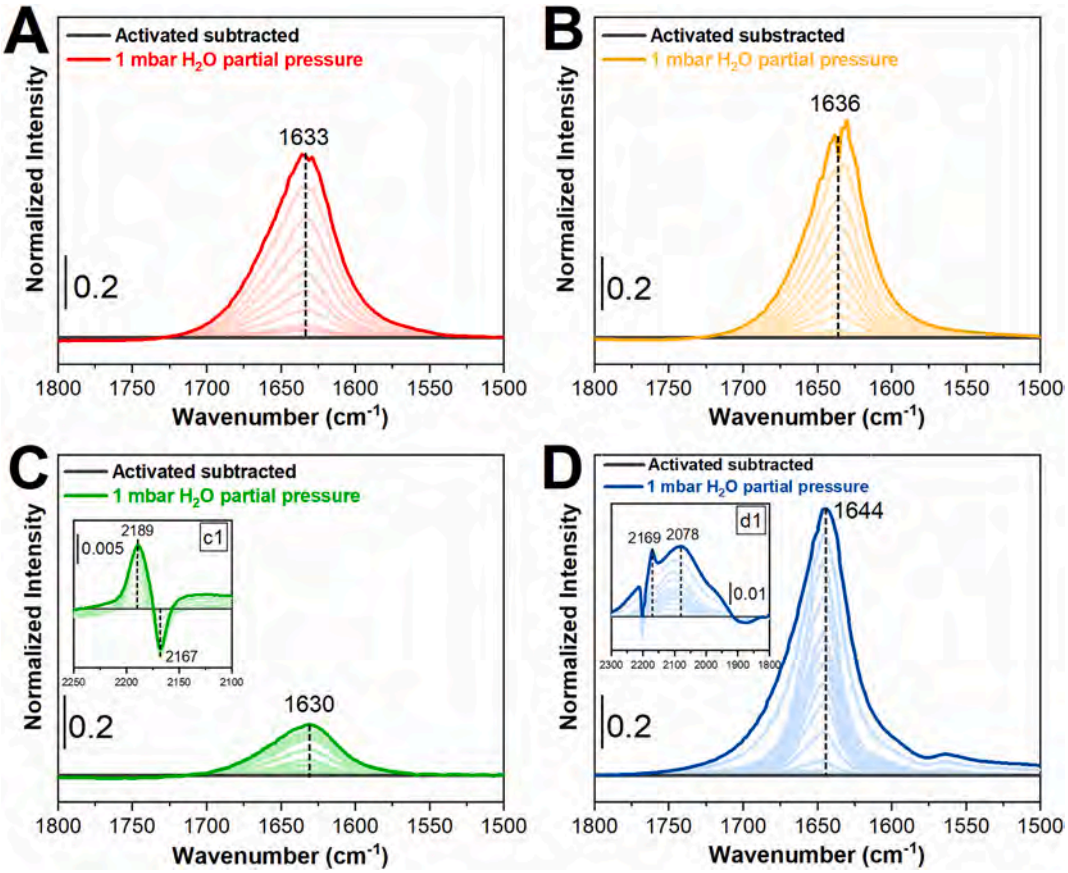

Fig. 10. In situ FTIR difference spectra of the water interacting region (1800–1500 cm^{-1}) acquired on Clino (A), Na/Clino_L (B), Na/Clino_H (C), and 13X (D) at increasing water partial pressure (from $9 \cdot 10^{-4}$ to 1 mbar). Magnifications of significant bands are shown in the insets. The bold black line represents the subtracted spectra obtained from materials activation; the bold colored line refers to 1 mbar water partial pressure.

corresponded to the split ν_3 vibrations of adsorbed NO_3^-. These assignments appeared more plausible, considering that the Na/Clino_H sample was functionalized using sodium nitrate precursors, which may have remained complexed with the metal [68,71,73]. However, no crystalline sodium nitrate phase was detected by XRD, suggesting that these signals are unlikely to originate from bulk $NaNO_3$ residues. Therefore, these bands are more plausibly associated with surface-adsorbed or strongly coordinated NOx-derived species formed during synthesis, ion exchange, or subsequent exposure to ambient atmosphere during sample handling.

The study of hydrophilic behavior concerning the content of alkali metal cations (in this case Na^+) is fundamental to understanding changes in zeolites' water adsorption capacity, which is not affected by Al (since EDX results showed that the Si/Al ratio and therefore Al content did not change so much with ion exchange). Concerning previous studies on this topic, it was found that unexchanged zeolites, especially at low pressures, tended to exhibit water clustering, which occurred when there was a stronger interaction between two water molecules with respect to the one within the water molecule and the adsorption site. It also came out that in the exchanged zeolites, on the contrary, water clustering is avoided by the stronger interaction between the sorbate molecule (water) and the exchanged cation, thus resulting in all water molecules bound to the zeolites' surface, utilizing the cation itself [18]. Therefore, ion exchange can alter the hydration environment within the zeolite framework by modifying the distribution and accessibility of extra-framework cations, thus affecting water adsorption behavior. The evolution of the water's peak in the -OH bending region can be observed in Fig. 10.

All samples analyzed showed an increase in the peak at 1644–1630 cm^{-1} spectral range, thus confirming the effectiveness of water adsorption at increasing partial pressures. The 13X zeolite exhibited the highest affinity for water among the tested samples. This material not only demonstrated a more intense water bending signal at 1644 cm^{-1} but also displayed absorbance features within the 2300–1800 cm^{-1} spectral range, which increased with rising water pressure. The pronounced difference in the water bending absorption was attributed to the zeolite's notably high specific surface area (approximately twenty times greater than that of clinoptilolite-based materials) and its substantial sodium content (discussed above). Additionally, the hydrophobicity or hydrophilicity of the material can be adjusted by modifying the Si/Al ratio. Water molecules preferentially adsorb in regions of the zeolite framework where charge separation occurs. Therefore, samples with lower Si/Al ratios, such as the 13X zeolite examined in this study, are known to interact more strongly with water and accommodate a greater quantity of water molecules. This behavior could be due to the increased number of negatively charged oxygen atoms within the framework, along with a higher density of compensating cations, which results in more regions exhibiting charge separation [74,75]. Regarding the signals at 2169 cm^{-1} and 2078 cm^{-1}, absorptions in this spectral region are typically attributed to a bend and libration water combination band [76]. This band may be associated with a high surface coverage of the zeolite by water molecules.

Further confirmation of the strong interaction between zeolite 13X and water arose from the analysis of the -OH stretching region (Fig. 11). As the amount of water increased, the spectrum of this material (Fig. 11D) displayed several signals that intensified, specifically two sharp high-frequency bands at 3690 cm^{-1} and 3660 cm^{-1}, along with two broad associated bands at 3383 cm^{-1} and 3227 cm^{-1}. Two intense signals eventually replaced these broad bands at 3277 cm^{-1} and 3132 cm^{-1}. The two sharp high-frequency bands may originate from different

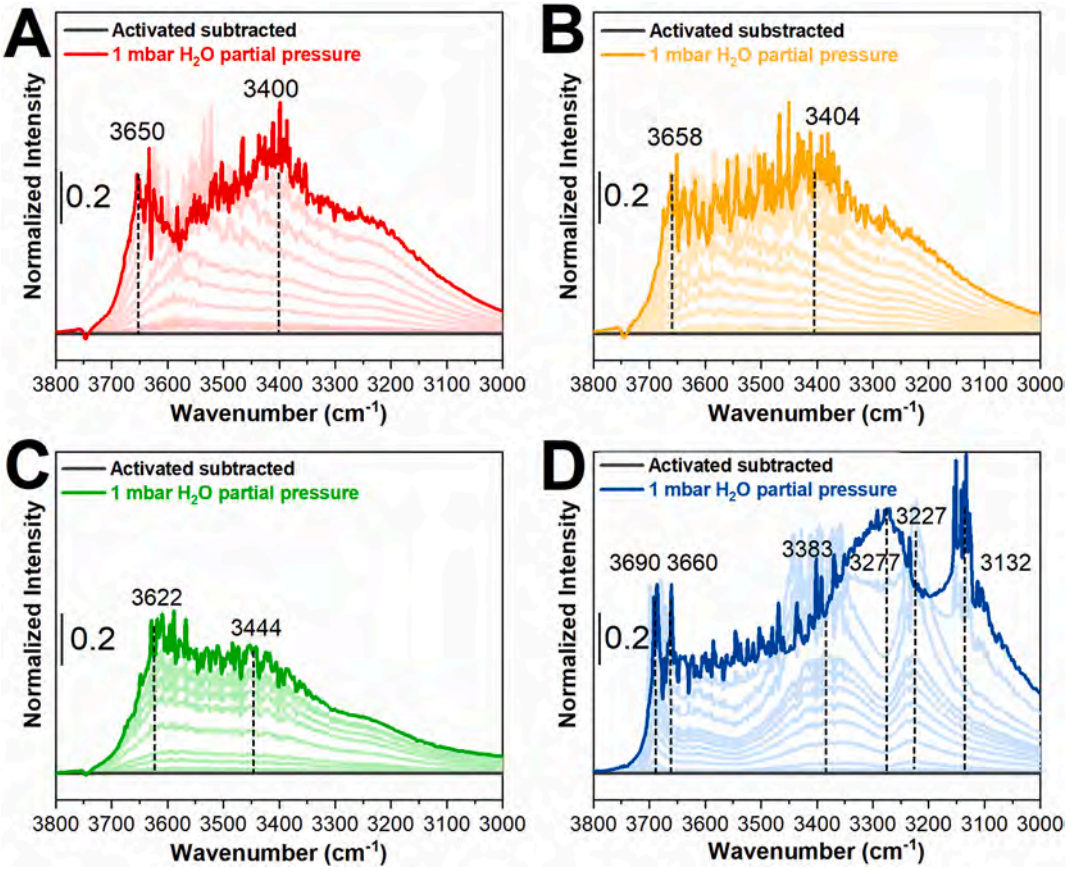

Fig. 11. In situ FTIR difference spectra of the water interacting region (3800–3000 cm^{-1}) acquired on Clino (A), Na/Clino_L (B), Na/Clino_H (C), and 13X (D) at increasing water partial pressure (from $9 \cdot 10^{-4}$ to 1 mbar). The bold black line represents the subtracted spectra obtained from materials activation; the bold colored line refers to 1 mbar water partial pressure.

water molecules located in two distinct positions within the zeolite cages, where one OH bond forms a hydrogen bond while the other OH bond remains free. These positions could correspond to different crystallographic sites (e.g., cages of different types) or identical cages with different local environments due to the distribution of Na^+ ions (which migrate more readily when water is adsorbed). The two broad bands can be associated with water molecules in identical positions. At maximum surface coverage, these two broad bands were subsequently replaced by the intense signals at 3277 cm^{-1} and 3132 cm^{-1}. The downshift of these signals indicated an increase in the average strength of hydrogen bonds among the adsorbed water molecules, thereby confirming a high degree of surface coverage [77].

Regarding clinoptilolite-based materials, their spectra exhibited very similar features both in the OH bending region (**Fig. 10A** and **B**) and in the silanol spectral region (**Fig. 11A** and **B**). The Clino and Na/Clino_L samples displayed comparable relative intensities, indicating that ion exchange has had a minimal impact on the performance of the bare clinoptilolite. The silanol region exhibited similar spectral characteristics for both samples, including an isolated OH stretching vibration of water at approximately 3650 cm^{-1}. A broad band around 3400 cm^{-1} was observed, which can be mainly associated with hydrogen-bonded OH species [78,79]. Although the samples were pretreated under high vacuum at 400 °C, contributions from strongly retained water molecules coordinated to extra-framework cations cannot be excluded.

Regarding the Na/Clino_H sample, the isolated silanol groups shifted to 3622 cm^{-1}, while the hydrogen-bonded OH groups displayed a broad band at 3444 cm^{-1}. A possible explanation for the downshift observed in the previous signal may be linked to a reduction in their number due to increased zeolite functionalisation by sodium species. Similarly, the band positioned at 3444 cm^{-1} might reflect a decrease in the number of water species interacting with each other.

The absorption at 1630 cm^{-1} exhibited a significantly lower relative intensity compared to other samples, despite the higher sodium loading. As previously mentioned, part of the sodium in this sample remained complexed with NO_x groups originating from the sodium precursor. Consequently, the lower water uptake observed for this sample could plausibly be attributed to a reduced number of metal centres available for water interaction. Additionally, extensive functionalisation may have partially covered the zeolite surface, further limiting H_2O-zeolite interactions. Following water introduction, an increase in the signal at 2189 cm^{-1} and a decrease at 2167 cm^{-1} were observed, as shown in inset c1 (Fig. 10C). A similar trend was reported by Szanyi et al. [71], where the intensity of the IR band corresponding to adsorbed NO^+ species (2053 cm^{-1}) diminished upon water addition and disappeared with higher water dosages. Interestingly, no change was noted in the intensity of the IR band attributed to the NO^+-NO_2 adduct. The authors proposed that this behavior arose from NO_2 within the NO^+-NO_2 adduct interacting strongly with NO^+, thereby shielding it from reacting with water. Conversely, NO^+ species remained vulnerable to attack by incoming water molecules.

The water adsorption phenomenon was more evident at higher pressures, where no overlapping between spectra was recorded. As a matter of fact, according to the literature [80], adsorption was more incentivized in partially hydrated samples because there was no interfacial mass transport phenomenon limiting step, as in the dried sample. Precisely, when the intergranular region was saturated by water (partially hydrated samples), the adsorption happened on the external surface, and it consisted of two steps involving the bond between the adsorbate (water) molecules and extra-framework cations. In particular, during the first slow step, water was captured by the electric field of the cations, thus leading to the formation of a water/cation adduct, whereas in the faster step, there was a rearrangement of water molecules at the cation-framework interface, which allowed the creation of hydrogen bonds and, consequently, the maximization of physical interactions [80]. It should be added that, as expected, synthetic 13X displayed a higher affinity with water than natural samples.

A superposition between spectra was quite evident in the case of time expansions, suggesting that it was possible to desorb water only through thermal expansion because of the strength of hydrogen bonds. However, the Na/Clino_H sample constituted the only exception. In fact, as can be observed in Fig. 12, this sample seemed to show a minor affinity with water, and this was supported by the fact that there was a downward trend of the peak centered at 1641 cm^{-1} during gradual time expansion, thus demonstrating that, in this case, desorption did not need thermal treatment.

Finally, Fig. 13 illustrates the comparison of water affinity between all the samples investigated. A clear correlation between the adsorption properties of the investigated zeolites was observed by comparing the results obtained from in situ FTIR spectroscopy with those from climatic chamber experiments conducted at varying levels of RH. Specifically, the FTIR signal intensity as a function of water vapor partial pressure (P_line) showed the same trend seen in the equilibrium mass loss measurements, which reflected the amount of water adsorbed under humid conditions. Both experiments demonstrated the same following trend: 13X > Na/Clino_L > Clino > Na/Clino_H.

Precisely, as expected, in both cases, zeolite 13X was the best-performing material due to its highly accessible porous structure and strong polarity, which facilitated more efficient water adsorption. The Na/Clino_L sample demonstrated intermediate performance, slightly superior to that of the untreated natural Clino, but lower than that of 13X. On the other hand, the highly sodium-exchanged clinoptilolite (Na/Clino_H) showed the lowest water uptake, suggesting that an excessive degree of cation exchange may reduce the accessibility of active adsorption sites or negatively impact the pore structure. These outcomes revealed that treating zeolites with high sodium concentrations appears to hinder water adsorption, while moderate sodium exchange slightly enhanced the capacity compared to the natural clinoptilolite. Consequently, the lower water uptake observed for Na/Clino_H sample could plausibly be attributed to a reduced number of metal centres available for water interaction. Additionally, extensive functionalization may have partially covered the zeolite surface, further limiting H_2O-zeolite interactions. In addition, the adsorption behavior of clinoptilolite is not solely governed by the total sodium content, but also by the crystallographic distribution and occupancy of extra-framework cationic sites, which may alter the available pore volume and accessibility for water molecules [81,82]. Excessive Na-exchange may therefore promote partial pore blocking or modifications in the local water adsorption environment, resulting in lower overall water uptake despite the increased sodium concentration.

To conclude, the water adsorption behavior of clinoptilolite-based materials can be rationalized by combining spectroscopic and gravimetric results. FT-IR analysis provided evidence that ion exchange modifies the local environment of framework-associated hydroxyl groups, affecting their interaction with water molecules. However, DVS measurements demonstrated that the overall water uptake is not directly proportional to sodium content. In particular, Na/Clino_L exhibited enhanced adsorption at high relative humidity, likely due to the development of additional accessible porosity, whereas Na/Clino_H showed reduced uptake, suggesting partial blocking of adsorption sites or reduced accessibility of cationic centers. Zeolite 13X, in contrast, combined high sodium content with a well-defined microporous FAU structure, resulting in the highest water uptake. These findings highlighted that water affinity is governed by a combined effect of cation distribution, framework accessibility, and pore architecture rather than by a single compositional parameter.

Overall, the FT-IR results provided molecular-level evidence that the variation in extra-framework cation content modulated the strength and nature of water-zeolite interactions, which was consistent with the macroscopic adsorption behavior observed in TGA, DSC, and climatic chamber experiments.

The combined experimental evidence highlighted that the variation in extra-framework Na^+ content, confirmed by EDX analysis, modified

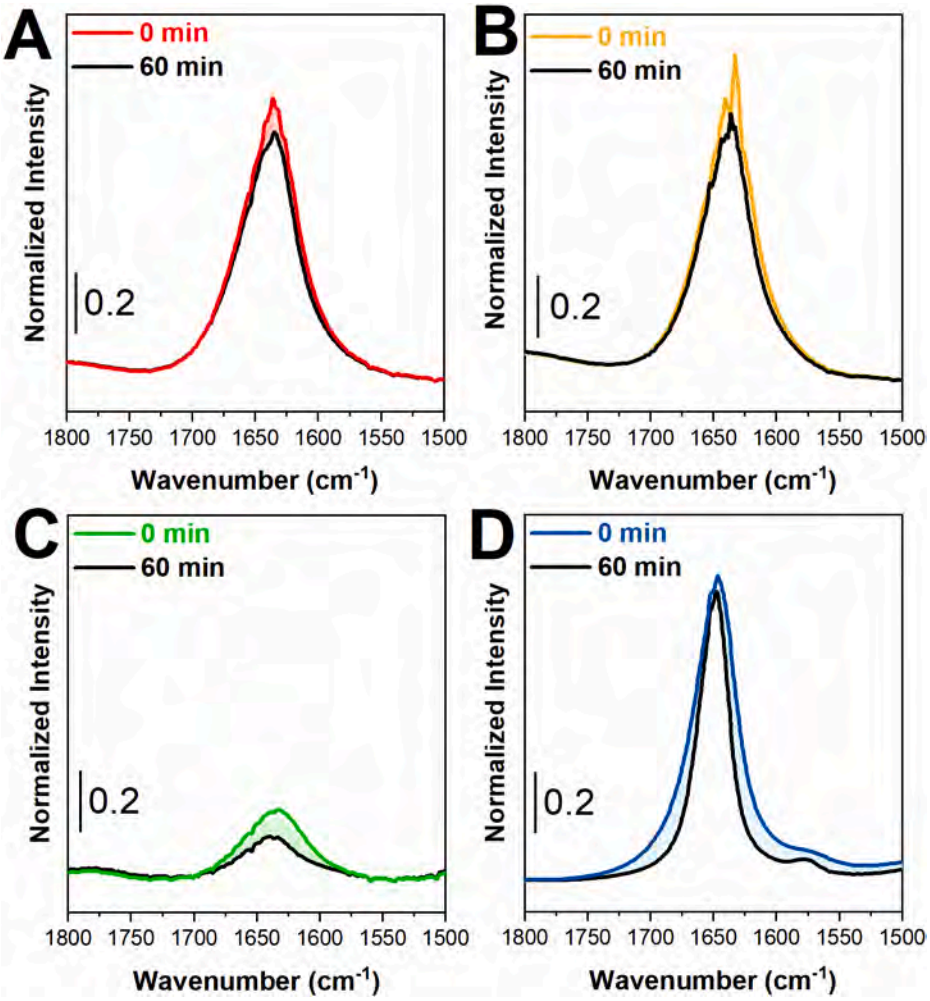

Fig. 12. Time-dependent degassing in situ FTIR spectra of the water interacting region (1800–1500 cm^{-1}) acquired on Clino (A), Na/Clino_L (B), Na/Clino_H (C), and 13X (D).

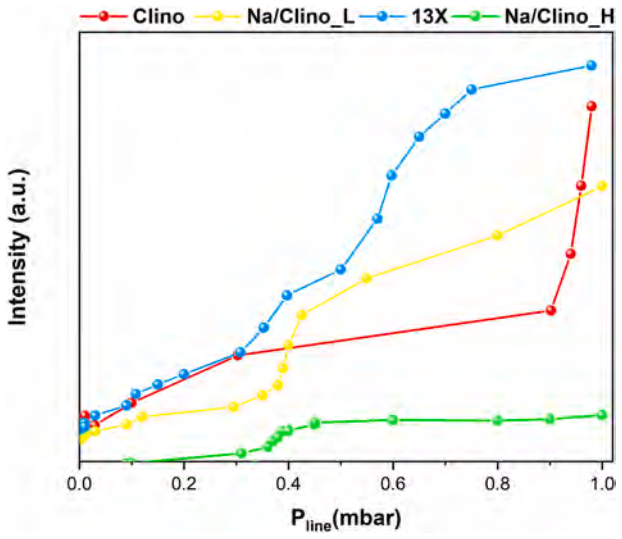

Fig. 13. Water affinity comparison resulted from FT-IR analysis for all the samples investigated.

the distribution and nature of charge-balancing sites within the zeolite framework. This compositional change was reflected at the molecular level by FT-IR spectroscopy, where systematic shifts in hydroxyl stretching bands indicated a progressive alteration between water molecules and adsorption sites. As a consequence, the strength and organization of the adsorbed water phase are affected, leading to measurable differences in water uptake and desorption behavior, as evidenced by thermogravimetric and dynamic sorption analyses. In particular, moderate sodium exchange enhanced the accessible adsorption sites and promoted stronger water-cation interactions, resulting in increased reversible water uptake, whereas excessive sodium loading appeared to partially hinder accessibility to the porous network and reduce overall adsorption efficiency. These molecular-level effects were directly translated into macroscopic thermal performance, as demonstrated by differential scanning calorimetry results and the resulting energy density values. Therefore, the observed variations in thermal energy storage capacity can be rationalized as the direct outcome of sodium-induced modifications in the zeolite-water interaction mechanism.

3.4. Key performance indicators (KPI) evaluation

As mentioned, the estimation of the KPI is essential to better investigate the performance of the samples investigated. Fig. 14 reports a graphical comparison among the four sorbent materials in terms of SCC and ED values, where the average price of the material (expressed in € ton^{-1}) was divided by the Energy Density, ED (kJ ton^{-1}), derived from the enthalpy estimated from DSC analysis. The SCC is a useful parameter

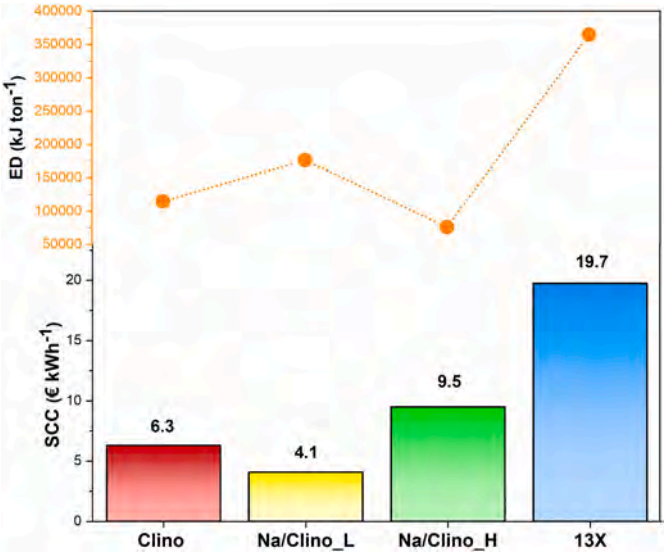

Fig. 14. SCC and ED evaluation for all the samples investigated.

for evaluating whether the material is competitive on a market scale, as an efficient but expensive adsorbent may not be suitable for implementation on a large scale. Therefore, it was fundamental to estimate the cost of both synthetic and natural zeolites. In this regard, it was worth emphasizing that synthetic zeolites are relatively more expensive than natural ones, as their synthesis requires the use of specialized equipment, pure substances, and energy. Among the synthetic zeolites, 13X is considered the cheapest. The most challenging part, however, was determining the exact price since this can vary depending on the supplier and the quantity purchased. The prices used in this study are intended as representative literature-based estimates rather than fixed market values, since no standardized or universally accepted pricing is available for these materials in literature or industrial databases. According to some market surveys, in 2015, the price of 13X was around 2750–3500 USD ton^{-1} (2000–3000 € ton^{-1} according to [22,23,80] and in some cases it peaked at 4354 USD ton^{-1} (6000 CAD ton^{-1}) [83]. Another recent study in 2022 reported that the market price for industrial quantities of zeolite 13X by a Chinese industry was around 1300–1800 USD ton^{-1} [20]. Based on these considerations, a price of 2000–3000 € ton^{-1} has been considered for the SCC calculation of 13X. It is also worth mentioning that synthetic 13X is not competitive from an economic point of view, if compared with other sorbents like bentonite or vermiculite (160 € ton^{-1}), and this negatively affects their SCC value [18]. Natural zeolite, on the other hand, represents abundant, low-cost natural minerals. Although their quality can be affected by impurities, their performance can be improved through functionalization. In this work, a market price of 200–300 € ton^{-1} for natural samples was considered, according to the literature [84]. It was evident that the difference in terms of price (of an order of magnitude) between these materials deeply influenced the SCC value. Therefore, the SCC was calculated for the four samples, and the outcome was compared with the SCC of the most common adsorbents from literature data.

From the results reported in Fig. 14, it can be observed that Na/Clino_L offered the most cost-effective solution, with the lowest SCC (4.1 € kWh^{-1}), despite having a moderate energy density. Clino also showed a relatively low SCC (6.3 € kWh^{-1}), making it a viable option in terms of cost.

On the other hand, 13X, although exhibiting the highest energy density, demonstrated the highest SCC (19.7 € kWh^{-1}), indicating that its superior energy performance came at a significantly higher cost. On the contrary, Na/Clino_H showed a moderate SCC (9.5 € kWh^{-1}) and relatively low ED, making it less attractive compared to Na/Clino_L.

Overall, the SCC analysis provided a preliminary indication that Na/Clino_L may represent a promising compromise between energy storage capacity and material cost among the investigated samples. However, further optimization and system-level investigations are required to fully assess its practical applicability in TES systems, while materials like 13X may be more suitable when energy density is prioritized over cost.

These results were consistent with the structural and adsorption properties discussed above, where moderate sodium exchange optimizes the balance between water uptake capacity and thermal stability, leading to improved overall energy storage performance.

The experimental results obtained showed that the ED and SCC values of the zeolites analyzed in this study were consistent with those of the main materials used in the energy field and TES systems, as shown in Table 3. To be precise, natural zeolites seem to be comparable in terms of costs to other natural minerals, such as Bentonite and Vermiculite, or composites (Vermiculite/$CaCl_2$), that are more cost-effective than SAPO or AlPO materials. However, these natural zeolites exhibited lower ED, which could offset the positive SCC value. Nevertheless, their physico-chemical properties can be tuned to make them a promising substitute for 13X and other synthetic zeolites. As an alternative, thanks to their porous structure as well as their good cation exchange capacity, they could be exploited as low-cost supports for salts (i.e., $CaCl_2$) to create composite materials in TES systems. Further investigations should be conducted in this context to evaluate the feasibility of substituting natural clinoptilolite with synthetic 13X.

4. Conclusions

The present study aimed to address a critical knowledge gap by systematically correlating the extra-framework cation composition of natural clinoptilolite with its molecular-scale water adsorption mechanisms and macroscopic thermal energy storage performance. Unlike previous studies that have primarily focused on either structural characterization or adsorption behavior in isolation, this work integrated complementary physico-chemical techniques to try to establish a direct structure-property-performance relationship. In particular, this work lies in the comprehensive multi-technique approach adopted to investigate how the concentration of exchangeable cations (specifically Na^+) affects the water sorption capacity of a natural zeolite clinoptilolite. In situ FT-IR spectroscopy provided molecular-level insights into water-zeolite interactions and the role of hydroxyl species and extra-framework cationic sites. These microscopic findings were then directly linked to macroscopic measurements obtained from TGA, DSC, and dynamic water sorption tests, enabling a comprehensive evaluation

Table 3
Comparison of the KPI of the existing materials.

Material	Energy density GJ ton^{-1}	SCC € kWh^{-1}	Cost € ton^{-1}	Ref.
13X	0.36	19.7	2000	This work
Clinoptilolite	0.11	6.3	200	This work
Na/Clino_L	0.18	4.1	200	This work
Na/Clino_H	0.07	9.5	200	This work
13X	0.39	18.52	2000	[85]
13X/$MgSO_4$	0.65	10.03	1805	[85]
Zeolite Y	–	26	1100	[18]
NaX zeolite	0.54	–	–	[86]
SAPO-34	0.73	985.22	200,000	[85]
SAPO 34	–	565	100,000	[18]
SAPO 34	0.85	–	–	[86]
AlPO-18	0.87	823.05	200,000	[85]
PC/$MgSO_4$	0.078	1.7	132.6	[85]
CSA/70%sep/ $MgSO_4$	0.084	9.4	212.4	[87]
Silica gel/$CaCl_2$	0.48	26.39	3843.50	[85]
Silica gel	0.3	–	–	[86]
Vermiculite/$CaCl_2$	1	1.18	329	[85]
Vermiculite/$CaCl_2$	–	0.4	1571	[18]
Vermiculite	–	8	160	[18]
Bentonite	–	2	170	[18]

of adsorption capacity, dehydration behavior, and energy storage potential. By integrating these multiscale characterizations, the study elucidated how controlled sodium exchange modulated hydrophilicity and thermal performance. The results revealed that a moderate sodium exchange improved hydrophilicity and adsorption performance, while excessive sodium content can negatively impact the material's porosity and water uptake. By tuning the sodium content, natural clinoptilolite can be optimized to achieve cost-effective thermal energy storage performance through controlled water adsorption behavior. Finally, thermal analysis, including TGA and DSC, allows for the evaluation of the Energy Density (ED) and consequently the specific cost capacity (SCC) of these materials, thus revealing that Na/Clino_L with its moderate sodium content, offered the most cost-effective solution, with a low cost (200 € ton^{-1}) and the lowest SCC value (4.1 € kWh^{-1}) which makes it comparable with the other conventional materials exploited in thermal energy sector.

These findings could represent a low-cost and scalable alternative to synthetic materials for future sorption-based TES systems, particularly in low-to-medium temperature applications.

CRediT authorship contribution statement

Nadia Grifasi: Conceptualization, Data curation, Formal analysis, Investigation, Methodology, Visualization, Writing – original and reviewed draft. **Bianca Ziantoni:** Data curation, Formal analysis, Investigation, Methodology, Visualization, Writing – original and reviewed draft. **Alessio Mondello:** Data curation, Formal analysis, Investigation, Methodology, Writing – original draft. **Giuseppe Cruciani:** Data curation, Formal analysis, Methodology, Writing – original draft. **Andrea Rizzetto:** Data curation, Formal analysis, Investigation, Methodology, Visualization, Writing – original draft. **Luca Lavagna:** Investigation, Methodology, Writing – original draft. **Matteo Pavese:** Supervision. **Fabio A. Deorsola:** Supervision. **Debora Fino:** Supervision. **Marco Piumetti:** Conceptualization, Supervision.

Declaration of competing interest

The authors declare that they have no known competing financial interests or personal relationships that could have appeared to influence the work reported in this paper.

Acknowledgement

The authors thank Camilla Galletti for XRD measurement and Marco Allione for EDX analyses.

Data availability

Data will be made available on request.

References

[1] H.K. Jeswani, S.Z. Boada, V. Spallina, A. Azapagic, Towards net-zero in steel production: process simulation and environmental impacts of carbon capture, storage and utilisation of blast furnace gas, Carbon Capture Sci. Technol. 15 (2025) 100387, https://doi.org/10.1016/j.ccst.2025.100387.
[2] G. Dhingra, A. Kumar, Carbon capture and sequestration: cutting-edge technologies to combat climate change, Sustain. Energy Techn. and Assess. 75 (2025) 104226.
[3] T.M. Thiedemann, M. Wark, A compact review of current technologies for carbon capture as well as storing and utilizing the captured CO2, Processes 13 (2025) 283.
[4] M. Cavallo, M. Dosa, N.G. Porcaro, F. Bonino, M. Piumetti, V. Crocella, Shaped natural and synthetic zeolites for CO2 capture in a wide temperature range, J. CO_2 Util. 67 (2023), https://doi.org/10.1016/j.jcou.2022.102335.
[5] E. Davarpanah, M. Armandi, S. Hernández, D. Fino, R. Arletti, S. Bensaid, M. Piumetti, CO2 capture on natural zeolite Clinoptilolite: effect of temperature and role of the adsorption sites, J. Environ. Manag. 275 (2020) 111229, https://doi.org/10.1016/j.jenvman.2020.111229.
[6] M. Dosa, M. Piumetti, E. Davarpanah, G. Moncaglieri, S. Bensaid, D. Fino, Natural Zeolites as Sustainable Materials for Environmental Processes, in: M. Piumetti, S. Bensaid (Eds.), Nanostructured Catalysts for Environmental Applications, Springer International Publishing, Cham, 2021, pp. 367–381. ISBN 978–3–030-58934-9.
[7] A. Rizzetto, M. Piumetti, R. Pirone, E. Sartoretti, S. Bensaid, Study of ceria-composite materials for high-temperature CO2 capture and their ruthenium functionalization for methane production, Catal. Today 429 (2024) 114478, https://doi.org/10.1016/j.cattod.2023.114478.
[8] A. Rizzetto, E. Sartoretti, M. Piumetti, R. Pirone, S. Bensaid, Novel application of Ru-based catalysts on MgAl oxides alkaline adsorbents for cyclic CO2 Methanation, Chem. Eng. J. 501 (2024) 157585.
[9] M. Pietro Mezzapesa, F. Salomone, H. Guzmán, F. Zammillo, R. Millini, L. Bua, G. Marra, A. Tacca, R. Marrazzo, N. Russo, Development of in–cu binary oxide catalysts for hydrogenating CO_2 via thermocatalytic and electrocatalytic routes, Inorg. Chem. Front. 11 (2024) 2319–2338.
[10] F. Salomone, E. Sartoretti, S. Ballauri, M. Castellino, C. Novara, F. Giorgis, R. Pirone, S. Bensaid, CO2 hydrogenation to methanol over Zr-and Ce-doped indium oxide, Catal. Today 423 (2023) 114023.
[11] H. Guzman, F. Salomone, E. Batuecas, T. Tommasi, N. Russo, S. Bensaid, S. Hernandez, How to make sustainable CO2 conversion to methanol: Thermocatalytic versus Electrocatalytic technology, Chem. Eng. J. 417 (2021) 127973.
[12] F. Salomone, P. Marocco, D. Ferrario, A. Lanzini, D. Fino, S. Bensaid, M. Santarelli, Process simulation and energy analysis of synthetic natural gas production from water electrolysis and CO2 capture in a waste incinerator, Appl. Energy 343 (2023) 121200.
[13] E. Corrao, F. Salomone, E. Giglio, M. Castellino, S.M. Ronchetti, M. Armandi, R. Pirone, S. Bensaid, CO2 conversion into hydrocarbons via modified Fischer-Tropsch synthesis by using bulk Iron catalysts combined with zeolites, Chem. Eng. Res. Des. 197 (2023) 449–465, https://doi.org/10.1016/j.cherd.2023.07.052.
[14] EPA United States Environmental Protection Agency Overview of Greenhouse Gases, Available online, https://www.epa.gov/ghgemissions/overview-greenhouse-gases, 2025. accessed on 14 June 2025.
[15] Hannah Ritchie, Max Roser, Global Carbon Budget, in: Global Carbon Project (Ed.), with Major Processing by Our World in Data, Annual CO_2 Emissions – GCB, 2023. "Global Carbon Budget". [Original Data]. Available online: https://ourworldindata.org/co2-emissions (accessed on 24 June 2024)..
[16] P.M. Haugan, H. Drange, Effects of CO2 on the ocean environment, Energy Convers. Manag. 37 (1996) 1019–1022, https://doi.org/10.1016/0196-8904(95)00292-8.
[17] K.O. Yoro, M.O. Daramola, in: M.R. Rahimpour, M. Farsi, M.A.B.T.-A. in C. C. Makarem (Eds.), Chapter 1 - CO2 Emission Sources, Greenhouse Gases, and the Global Warming Effect, Woodhead Publishing, 2020, pp. 3–28. ISBN 978–0–12-819657-1.
[18] L. Aghemo, L. Lavagna, E. Chiavazzo, M. Pavese, Comparison of key performance indicators of sorbent materials for thermal energy storage with an economic focus, Energy Storage Mater. 55 (2023) 130–153, https://doi.org/10.1016/j.ensm.2022.11.042.
[19] A. Kalair, N. Abas, M.S. Saleem, A.R. Kalair, N. Khan, Role of energy storage systems in energy transition from fossil fuels to renewables, Energy Storage 3 (2021) e135.
[20] B. de Gennaro, A. Cappi, M. de Gennaro, N. Bianco, A. Langella, P. Cappelletti, A. Marocco, P. Aprea, M. Pansini, Use of zeolites in the capture and storage of thermal energy by water desorption—adsorption cycles, Materials (Basel, Switzerland) 15 (2022) 5574.
[21] K. Kant, R. Pitchumani, Advances and opportunities in thermochemical heat storage Systems for Buildings Applications, Appl. Energy 321 (2022) 119299, https://doi.org/10.1016/j.apenergy.2022.119299.
[22] V. Palomba, A. Frazzica, Recent advancements in sorption technology for solar thermal energy storage applications, Sol. Energy 192 (2019) 69–105, https://doi.org/10.1016/j.solener.2018.06.102.
[23] L. Kouchachvili, D.A. Bardy, R. Djebbar, L.E.W. Hogg, Natural zeolites as host matrices for the development of low-cost and stable thermochemical energy storage materials, J. Porous. Mater. 30 (2023) 163–173.
[24] P.A.J. Donkers, L.C. Sögütoglu, H.P. Huinink, H.R. Fischer, O.C.G. Adan, A review of salt hydrates for seasonal heat storage in domestic applications, Appl. Energy 199 (2017) 45–68.
[25] D.I. Tchernev, Solar Energy Application of Natural Zeolites, in: Natural Zeolites—Occurrence, Properties, *Use*, **1978**.
[26] C. Feng, E. Jiaqiang, W. Han, Y. Deng, B. Zhang, X. Zhao, D. Han, Key technology and application analysis of zeolite adsorption for energy storage and heat-mass transfer process: a review, Renew. Sust. Energ. Rev. 144 (2021) 110954.
[27] N. Grifasi, B. Ziantoni, D. Fino, M. Piumetti, Fundamental properties and sustainable applications of the natural zeolite clinoptilolite, Environ. Sci. Pollut. Res. Int. (2024), https://doi.org/10.1007/s11356-024-33656-5.
[28] N. Grifasi, M. Fornaro, M. Piumetti, B. Liguori, D. Caputo, Chromium recovery from tannery wastewater by zeolite-based materials: A circular and sustainable approach, in: Advanced Technologies in Wastewater Treatment, Elsevier, 2025, pp. 243–261.
[29] K. Narwal, S. Farsad, R. Kempers, P.G. O'Brien, Adsorption-based thermal energy storage using zeolites for mobile heat transfer, Energy Storage 6 (2024) e70041.
[30] S. Hongois, F. Kuznik, P. Stevens, J.-J. Roux, Development and characterisation of a new MgSO4– zeolite composite for long-term thermal energy storage, Sol. Energy Mater. Sol. Cells 95 (2011) 1831–1837.
[31] Y. Zhang, R. Wang, Sorption thermal energy storage: concept, process, applications and perspectives, Energy Storage Mater. 27 (2020) 352–369.
[32] K. Johannes, F. Kuznik, J.-L. Hubert, F. Durier, C. Obrecht, Design and characterisation of a high powered energy dense zeolite thermal energy storage

system for buildings, Appl. Energy 159 (2015) 80–86, https://doi.org/10.1016/j.apenergy.2015.08.109.
[33] S. De Antonellis, L.P.M. Colombo, P. Castellazzi, A. Rossetti, L. Marocco, System integration analysis of a zeolite 13x thermal energy storage, Energy and Built Environment 5 (2024) 568–579, https://doi.org/10.1016/j.enbenv.2023.04.006.
[34] S. Sultana, A. Pal, K.A. Rocky, A. Kowsar, I.M. Syed, B.B. Saha, Thermodynamic study of zeolite and graphene Nanoplatelet-based composites for Adsorption cooling systems, Appl. Therm. Eng. 254 (2024) 123850, https://doi.org/10.1016/j.applthermaleng.2024.123850.
[35] D. Mahon, G. Claudio, P.C. Eames, An experimental investigation to assess the potential of using MgSO4 impregnation and Mg2+ ion exchange to enhance the performance of 13X molecular sieves for interseasonal domestic thermochemical energy storage, Energy Convers. Manag. 150 (2017) 870–877.
[36] S.Z. Xu, R.Z. Wang, L.W. Wang, J. Zhu, A zeolite 13X/magnesium sulfate–water sorption thermal energy storage device for domestic heating, Energy Convers. Manag. 171 (2018) 98–109.
[37] O. Korkuna, R. Leboda, J. Skubiszewska-Zięba, T. Vrublevs'ka, V.M. Gun'ko, J. Ryczkowski, Structural and physicochemical properties of natural zeolites: clinoptilolite and mordenite, Microporous Mesoporous Mater. 87 (2006) 243–254, https://doi.org/10.1016/j.micromeso.2005.08.002.
[38] R. Roque-Malherbe, Applications of natural zeolites in pollution abatement and industry, 2001, pp. 495–522.
[39] S. Yamanaka, P.B. Malla, S. Komarneni, Water sorption and desorption isotherms of some naturally occurring zeolites, Zeolites 9 (1989) 18–22.
[40] D.A. White, R.L. Bussey, Water sorption properties of modified Clinoptilolite, Sep. Purif. Technol. 11 (1997) 137–141.
[41] D.L. Bish, Effects of exchangeable cation composition on the thermal expansion/contraction of Clinoptilolite, Clay Clay Miner. 32 (1984) 444–452.
[42] Y.I. Tarasevich, I.G. Polyakova, V.E. Polyakov, Microcalorimetric study of the interaction between water and cation-substituted clinoptilolites, Colloid. J. 65 (2003) 493–499.
[43] P. Aprea, B. De Gennaro, N. Gargiulo, A. Peluso, B. Liguori, F. Iucolano, D. Caputo, Sr-, Zn-and cd-exchanged Zeolitic materials as water vapor adsorbents for thermal energy storage applications, Appl. Therm. Eng. 106 (2016) 1217–1224.
[44] S. Yang, A. Navrotsky, Energetics of formation and hydration of ion-exchanged zeolite Y, Microporous Mesoporous Mater. 37 (2000) 175–186.
[45] N. Nasruddin, A.P. Arsyad, D. Djubaedah, D.A. Wulandari, H.F. Hidayat, Experimental Analysis of Indonesian Natural Zeolites-Water Pair for Closed System Adsorption Thermal Energy Storage, Proceedings of the AIP Conference Proceedings, AIP Publishing, 2020. Vol. 2255.
[46] L. Mihaly-Cozmuta, A. Mihaly-Cozmuta, A. Peter, C. Nicula, H. Tutu, D. Silipas, E. Indrea, Adsorption of heavy metal cations by Na-Clinoptilolite: equilibrium and selectivity studies, J. Environ. Manag. 137 (2014) 69–80, https://doi.org/10.1016/j.jenvman.2014.02.007.
[47] S. Ballauri, E. Sartoretti, M. Hu, C. D'Agostino, Z. Ge, L. Wu, C. Novara, F. Giorgis, M. Piumetti, D. Fino, Praseodymium doping in ceria-supported palladium nanocatalysts as an effective strategy to minimize the inhibiting effects of water during methane oxidation, Appl. Catal. B 320 (2023) 121898.
[48] E. Sartoretti, C. Novara, M.C. Paganini, M. Chiesa, M. Castellino, F. Giorgis, M. Piumetti, S. Bensaid, D. Fino, N. Russo, Investigation of cu-doped ceria through a combined spectroscopic approach: involvement of different catalytic sites in CO oxidation, Catal. Today 420 (2023) 114037, https://doi.org/10.1016/j.cattod.2023.02.014.
[49] P. Kowalczyk, M. Sprynskyy, A.P. Terzyk, M. Lebedynets, J. Namieśnik, B. Buszewski, Porous structure of natural and modified Clinoptilolites, J. Colloid Interface Sci. 297 (2006) 77–85.
[50] I. Rodríguez-Iznaga, M.G. Shelyapina, V. Petranovskii, Ion exchange in natural Clinoptilolite: aspects related to its structure and applications, Minerals 12 (2022) 1628.
[51] V. Tejavath, V. Kasarabada, S. Gonuguntla, V. Perupoga, S.V. Nandury, S. Bojja, U. Pal, Technoeconomic investigation of amine-grafted zeolites and their kinetics for CO2 capture, ACS Omega 6 (2021) 6153–6162.
[52] C. Ramakrishna, B.K. Saini, K. Racharla, S. Gujarathi, C.S. Sridara, A. Gupta, G. Thakkallapalli, P.V.L. Rao, Rapid and complete degradation of sulfur mustard adsorbed on M/zeolite-13X supported (M= 5 Wt% Mn, Fe, co) metal oxide catalysts with ozone, RSC Adv. 6 (2016) 90720–90731.
[53] M. Dosa, N. Grifasi, C. Galletti, D. Fino, M. Piumetti, Natural zeolite Clinoptilolite application in wastewater treatment: methylene blue, zinc and cadmium abatement tests and kinetic studies, Materials 15 (2022), https://doi.org/10.3390/ma15228191.
[54] M. Dosa, M. Piumetti, S. Bensaid, N. Russo, O. Baglieri, F. Miglietta, D. Fino, Properties of the clinoptilolite: characterization and adsorption tests with methylene blue, Journal of Advanced Catalysis Science and Technology 5 (2018) 1–10.
[55] L. Dimowa, N. Petrova, Y. Tzvetanova, O. Petrov, I. Piroeva, Structural features and thermal behavior of ion-exchanged clinoptilolite from Beli Plast deposit (Bulgaria), Minerals 12 (2022) 1576.
[56] G. Cruciani, Zeolites upon heating: factors governing their thermal stability and structural changes, J. Phys. Chem. Solids 67 (2006) 1973–1994.
[57] B. Alver, M. Sakizci, E. Yörükoğullari, Investigation of clinoptilolite rich natural zeolites from Turkey: a combined XRF, TG/DTG, DTA and DSC study, J. Therm. Anal. Calorim. 100 (2010) 19–26.
[58] P. Castaldi, L. Santona, C. Cozza, V. Giuliano, C. Abbruzzese, V. Nastro, P. Melis, Thermal and spectroscopic studies of zeolites exchanged with metal cations, J. Mol. Struct. 734 (2005) 99–105.
[59] G.D. Knowlton, T.R. White, H.L. McKague, Thermal study of types of water associated with clinoptilolite, Clay Clay Miner. 29 (1981) 403–411.
[60] T. Stanimirova, N. Petrova, G. Kirov, Comparative multi-stage TG-DSC study of K+, Na+, Ca2+ and Mg2+−exchanged clinoptilolite forms, Molecules 30 (2025) 4770.
[61] M. Thommes, K. Kaneko, A.V. Neimark, J.P. Olivier, F. Rodriguez-Reinoso, J. Rouquerol, K.S.W. Sing, Physisorption of gases, with special reference to the evaluation of surface area and pore size distribution (IUPAC technical report) 87 (2015) 1051–1069, https://doi.org/10.1515/pac-2014-1117.
[62] A. Rizzetto, E. Sartoretti, K. Khoma, M. Armandi, M. Piumetti, S. Bensaid, R. Pirone, The oscillatory behaviour of Cu-ZSM-5 catalysts for N_2O decomposition: investigation of Cu species by complementary techniques, ChemPhysChem 25 (15) (2024) e202400339, https://doi.org/10.1002/cphc.202400339.
[63] C. Lamberti, A. Zecchina, E. Groppo, S. Bordiga, Probing the surfaces of heterogeneous catalysts by in situ IR spectroscopy, Chem. Soc. Rev. 39 (2010) 4951–5001.
[64] E. Borfecchia, K.A. Lomachenko, F. Giordanino, H. Falsig, P. Beato, A.V. Soldatov, S. Bordiga, C. Lamberti, Revisiting the nature of Cu sites in the activated Cu-SSZ-13 catalyst for SCR reaction, Chem. Sci. 6 (2015) 548–563.
[65] S. Bordiga, C. Lamberti, F. Bonino, A. Travert, F. Thibault-Starzyk, Probing zeolites by vibrational spectroscopies, Chem. Soc. Rev. 44 (2015) 7262–7341.
[66] K. Chakarova, S. Andonova, L. Dimitrov, K. Hadjiivanov, FTIR study of CO and N2 Adsorption on [Ge] FAU zeolites in their Na-and H-forms, Microporous Mesoporous Mater. 220 (2016) 188–197.
[67] W. Wu, E. Weitz, Modification of acid sites in ZSM-5 by ion-exchange: an in-situ FTIR study, Appl. Surf. Sci. 316 (2014) 405–415.
[68] K. Naderi, F. Bahmanzadegan, B. Parizad, A. Ghaemi, S. Shahhosseini, Comprehensive analysis of O2 and N2 Adsorption on kaolin-derived zeolites: experimental and computational insights, Ind. Eng. Chem. Res. 63 (2024) 16061–16076.
[69] C. Cocuzza, G. Pietricola, I. Zonca, M. Dosa, O. Romero, T. Tommasi, V. Cauda, D. Fino, C. Ottone, M. Piumetti, Simultaneous CO 2 reduction and NADH regeneration using Formate and glycerol dehydrogenase enzymes co-immobilized on modified natural zeolite, RSC Adv. 12 (2022) 31142–31155.
[70] T. Montanari, G. Busca, On the mechanism of Adsorption and separation of CO2 on LTA zeolites: an IR investigation, Vib. Spectrosc. 46 (2008) 45–51.
[71] J. Szanyi, J.H. Kwak, C.H.F. Peden, The effect of water on the Adsorption of NO2 in Na− and Ba− Y, FAU zeolites: a combined FTIR and TPD investigation, J. Phys. Chem. B 108 (2004) 3746–3753.
[72] K. Khivantsev, N.R. Jaegers, H.A. Aleksandrov, L. Kovarik, M.A. Derewinski, Y. Wang, G.N. Vayssilov, J. Szanyi, Biomimetic CO oxidation below− 100 C by a nitrate-containing metal-free microporous system, Nat. Commun. 12 (2021) 6033.
[73] F.M. Higgins, N.H. de Leeuw, S.C. Parker, Modelling the effect of water on cation exchange in zeolite a, J. Mater. Chem. 12 (2002) 124–131.
[74] M.C. Bacariza, I. Graça, J.M. Lopes, C. Henriques, Tuning zeolite properties towards CO2 Methanation: an overview, ChemCatChem 11 (2019) 2388–2400.
[75] Z. Tahraoui, H. Nouali, C. Marichal, P. Forler, J. Klein, T.J. Daou, Influence of the compensating cation nature on the water adsorption properties of zeolites, Molecules 25 (2020) 944.
[76] P.K. Verma, A. Kundu, M.S. Puretz, C. Dhoonmoon, O.S. Chegwidden, C. H. Londergan, M. Cho, The bend+ libration combination band is an intrinsic, collective, and strongly solute-dependent reporter on the hydrogen bonding network of liquid water, J. Phys. Chem. B 122 (2017) 2587–2599.
[77] J. Hunger, I.A. Beta, H. Böhlig, C. Ling, H. Jobic, B. Hunger, Adsorption structures of water in NaX studied by DRIFT spectroscopy and neutron powder diffraction, J. Phys. Chem. B 110 (2006) 342–353.
[78] R. Kukobat, R. Škrbić, P. Massiani, K. Baghdad, F. Launay, M. Sarno, C. Cirillo, A. Senatore, E. Salčin, S.G. Atlagić, Thermal and structural stability of microporous natural Clinoptilolite zeolite, Microporous Mesoporous Mater. 341 (2022) 112101, https://doi.org/10.1016/j.micromeso.2022.112101.
[79] E.P. Favvas, C.G. Tsanaktsidis, A.A. Sapalidis, G.T. Tzilantonis, S.K. Papageorgiou, A.C. Mitropoulos, Clinoptilolite, a natural zeolite material: structural characterization and performance evaluation on its dehydration properties of hydrocarbon-based fuels, Microporous Mesoporous Mater. 225 (2016) 385–391, https://doi.org/10.1016/j.micromeso.2016.01.021.
[80] G. Carotenuto, C. Camerlingo, Kinetic investigation of water Physisorption on natural Clinoptilolite at room temperature, Microporous Mesoporous Mater. 302 (2020) 110238.
[81] G. Maurin, P. Llewellyn, T. Poyet, B. Kuchta, Influence of extra-framework cations on the Adsorption properties of X-Faujasite systems: microcalorimetry and molecular simulations, J. Phys. Chem. B 109 (2005) 125–129.
[82] Y. Garcia-Basabe, A.R. Ruiz-Salvador, G. Maurin, L.-C. de Menorval, I. Rodriguez-Iznaga, A. Gomez, Location of extra-framework Co2+, Ni2+, Cu2+ and Zn2+ cations in natural and Dealuminated Clinoptilolite, Microporous Mesoporous Mater. 155 (2012) 233–239.
[83] T.V. Tran, A.O. Oni, E. Gemechu, Y. Carrier, F.H. Tezel, A. Kumar, Developing a techno-economic model to evaluate the cost performance of a zeolite 13X-based space heating system, Energy Convers. Manag. 244 (2021) 114325.
[84] J. Jänchen, T. Herzog, E. Thrun, NATURAL ZEOLITES IN THERMAL ADSORPTION STORAGE AND BUILDING MATERIALS FOR SOLAR ENERGY UTILIZATION IN HOUSES, 2015.

[85] L. Lavagna, D. Burlon, R. Nisticò, V. Brancato, A. Frazzica, M. Pavese, E. Chiavazzo, Cementitious composite materials for thermal energy storage applications: a preliminary characterization and theoretical analysis, Sci. Rep. 10 (2020) 12833.
[86] H. Ayaz, V. Chinnasamy, J. Yong, H. Cho, Review of technologies and recent advances in low-temperature sorption thermal storage systems, Energies 14 (2021) 6052.
[87] S. Salustro, L. Lavagna, V. Fernicola, D. Smorgon, A. Mondello, E. Chiavazzo, M. Pavese, Thermal characterization and cost analysis of cement-based composite materials for thermochemical energy storage, J. Energy Storage 93 (2024) 112308.